To the Graduate Council:

I am submitting herewith a dissertation written by Jane Katherine Gates Jinkins entitled "The Analysis of Nonfluorescent Compounds by Electron Impact- and Laser Photolysis-Fragmentation Fluorescence Spectrometry." I have examined the final copy of this dissertation for form and content and recommend that it be accepted in partial fulfillment of the requirements for the degree of Doctor of Philosophy, with a major in Chemistry.

E. L. Wehry, Major Professor

We have read this dissertation and recommend its acceptance:

Accepted for the Council:

Vice Provost
and Dean of The Graduate School

THE ANALYSIS OF NONFLUORESCENT COMPOUNDS BY ELECTRON IMPACT- AND LASER PHOTOLYSIS-FRAGMENTATION FLUORESCENCE SPECTROMETRY

A Dissertation

Presented for the

Doctor of Philosophy

Degree

The University of Tennessee, Knoxville

Jane Katherine Gates Jinkins

December 1988

DEDICATION

This dissertation is dedicated to the author's parents, Mr. and Mrs Paul E. Gates; sisters Paula, Sherry, Carol, and Sue Ellen; and husband Bob, for their unwavering support and patience throughout her years in Graduate School.

ACKNOWLEDGMENTS

The author would like to acknowledge her appreciation of the technical assistance and guidance from the following individuals, each of whose contribution has been vital to the success of these experiments: Joel Alley, Priscilla J. Gannicott, Lauralee Guilbault, J. W. Gurley, Brian MacDonald, Ronald Hohmann, and John Schendel. Appreciation is also extended to Professor E. L. Wehry whose ideas are represented in this work.

The author would like to acknowledge the following members of the faculty for their help in reviewing this dissertation: E. L. Wehry, J. Q. Chambers, R. N. Compton, R. Pagni, and D. W. Weeter.

ABSTRACT

The development of alternative, fluorescence-based analytical techniques is being driven by two important properties of conventional fluorometric techniques; one, the characteristically low limits of detection obtainable for intensely fluorescent compounds and, two, the relatively small number of compounds possessing high quantum yields for fluorescence.

Small molecules, e.g., diatomics, triatomics, and atoms, are known to be intensely luminescent. Fragmentation Fluorescence Spectrometry (FFS) is a technique that takes advantage of this property and the fact that virtually any organic or organometallic compound can be broken into small molecular fragments. In the work presented in this dissertation, fragmentation of gas-phase molecules is accomplished through either the absorption of photons by laser photolysis (LP) or electron-impact bombardment (EI). The fluorescence is measured directly and related to the original amount of the parent compound.

In the following document, quantitative analyses (limits of detection, linear dynamic range, and precision) were carried out on a number of individual compounds by both EI- and LP-FFS. The detection limits of ammonia by EI- and LP-FFS were 20 pmol and 3.4 pmol, respectively. The compounds methylamine and acetonitrile were also analyzed using both techniques, with detection limits by EI of 0.3 nmol and 0.1 nmol, respectively, and by LP, 15 pmol, for methylamine. Acetonitrile did not produce fluorescent fragments under these

conditions of laser photolysis. Linear behavior was typical (2-3 decades) with the exception of ammonia in LP-FFS. Measurements made by EI-FFS are more reproducible than those of LP-FFS. Analytical precision as expressed by percent relative standard deviation was typically <1.5% for EI- and ~6% for LP-FFS.

The analysis of a series of aliphatic amines by LP-FFS indicated that detection limits do not dramatically increase for amines of higher molecular weights.

Studies of the use of a second laser with LP-FFS in a "photolysis-probe" arrangement to excite additional fluorescence from molecular fragments are described. No enhancement of fragment fluorescence was observed under the experimental conditions of this study.

TABLE OF CONTENTS

LIST OF TABLES

LIST OF FIGURES

CHAPTER I

INTRODUCTION

A. Molecular Fluorescence Spectrometry as a Method of Analysis

Molecular luminescence is a phenomenon whereby molecules are first electronically excited by the absorption of energy, followed by the loss of their excess energy through the emission of light. Molecular fluorescence is the term used to describe the study of luminescence that is derived from molecules that have been electronically excited. The energy necessary to induce electronic excitation of most organic molecules is on the order of 50-150 Kcal/mole; thus, electronic absorption and emission spectra are usually found in the UV or visible region of the electromagnetic spectrum (1).

1. Electronic Transitions in Molecules

Upon being excited to higher lying electronic states, a molecule may also be vibrationally excited. Molecules in condensed phases can lose excess vibrational energy by transferring it to other molecules through collisions. The energy is thus dissipated to the surroundings in the form of heat. Vibrational relaxation is a nonradiative process that occurs rapidly (10^{-12} s) and takes the molecule to the lowest vibrational level of the excited electronic state initially produced (2). The subsequent decay of an electronically excited molecule to the ground state can occur through more than one mechanism. These deexcitation processes are illustrated by Figure 1.

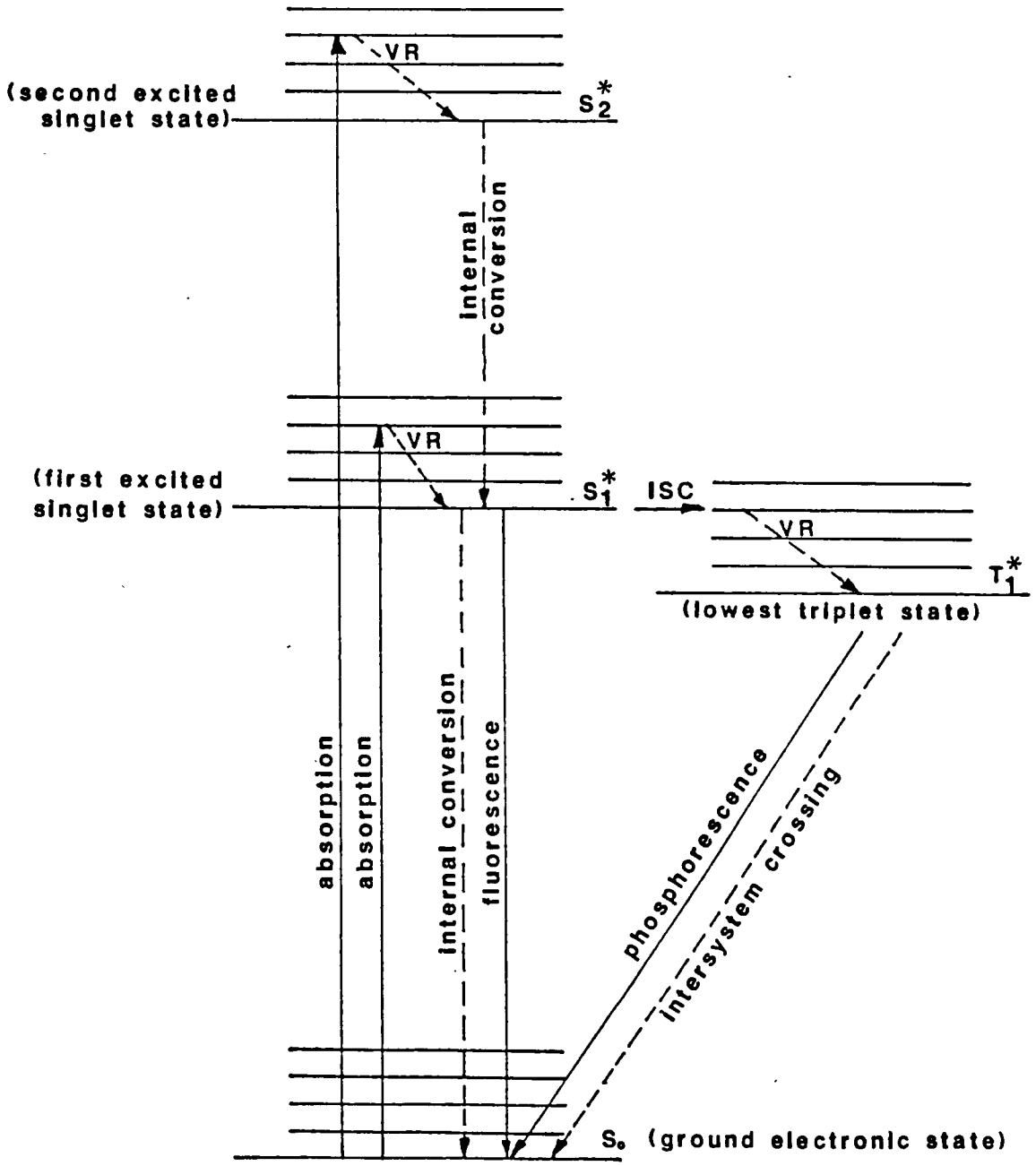

Figure 1. Schematic energy level diagram for molecular excitation and deexcitation processes. VR = vibrational relaxation; ISC = intersystem crossing. Solid arrows denote radiative processes; dashed arrows denote nonradiative processes.

Nonradiative deexcitation that does not involve a change in the spin state of the molecule is referred to as internal conversion; as is the case for vibrational relaxation, the excitation energy is dissipated as heat (2). The rate of internal conversion tends to be inversely proportional to the difference in energy between the excited state in question and the ground electronic state.

If there is any vibrational coupling between the lowest excited singlet state, S_1, and lowest triplet state, T_1, of a molecule, there exists the potential for nonradiative decay of S_1 to T_1. This process, known as intersystem crossing, produces molecules that are available to undergo radiative deexcitation back to the ground state. Luminescence originating from a triplet electronic state is called "phosphorescence." Phosphorescence occurs with a low probability since spin-reversal must occur a second time in order for there to be radiative emission from this state. Since phosphorescence depends upon a spin-forbidden process, triplet states can exhibit lifetimes from 10^{-4} to 10 s (1).

An alternate path for radiative deexcitation of condensed-phase molecules in S_1 is via molecular fluorescence. Fluorescence usually occurs from the lowest vibrational level of the lowest excited singlet state to any of the vibrational levels of the ground state. The energy differences associated with each transition reflects the differences in frequency of the corresponding vibrational levels of the ground state (1). Hence, the fluorescence resulting from each vibronic transition occurs at a specific wavelength and the fluorescence spectrum is

red-shifted, or occurs at higher wavelengths, relative to the corresponding absorption spectrum. Fluorescence lifetimes are relatively short (10^{-9}-10^{-7} s); thus, fluorescence competes with other deexcitation processes such as internal conversion or intersystem crossing (1). In general, the rates of radiative processes must be rapid relative to those of nonradiative processes in order for intense luminescence to be observed (3).

2. Analytical Advantages of Fluorescence Spectrometry

There are a number of significant analytical advantages of conventional molecular fluorescence spectrometry. Meaningful qualitative information can be derived from fluorescent molecules in terms of both emission (constant excitation λ) and excitation (constant emission λ) spectra, polarization studies and fluorescence decay times. Thus, fluorescence measurement techniques can be quite specific in nature, minimizing the amount of sample pretreatment.

As a quantitative method of chemical analysis, fluorescence measurements performed in solutions are highly sensitive (low parts per trillion (1)). Such low detection limits are due to two reasons. First, the difference between the wavelength of excitation and the wavelength of emission results in high discrimination against stray and scattered source radiation. This results in very low levels of background signal. Second, there exists a linear dependence of fluorescence intensity on the power of the source radiation (1).

Fluorescence signals can be enhanced by using more powerful excitation sources, the so-called "fluorescence advantage."

In addition, fluorescence detection can be accomplished in very small volumes, such as in high performance liquid chromatography or electrophoretic analysis; absolute detection limits of 0.01-1 pmol have been reported (4). Detection limits of luminescence techniques can be from one to four orders of magnitude lower than corresponding detection limits based on absorption. For example, fluorescence-based liquid chromatographic detection is, generally speaking, one to three orders of magnitude more sensitive than detection based on UV-vis absorption (4).

Fluorescence intensities often are linear in analyte concentration. In solution measurements, the fluorescence signal is typically found to be linear in concentration for at least two decades (1). The signal linearity is limited at low concentrations by "blank fluorescence" while at high concentrations negative deviations in linearity are likely to be due to self-absorption phenomena. Self-absorption occurs when the radiation emitted by one analyte molecule is reabsorbed by another analyte molecule.

3. Disadvantages of Fluorescence Spectrometry

The most significant limitation to conventional molecular fluorometry is that most molecules do not fluoresce efficiently. A general requirement for luminescence is that the molecule possess a high absorption coefficient, ϵ, for an electronic transition which

leads to the population of S_1 (3). It is also important, in order to reduce the likelihood of photodecomposition, that the electronic transition not be strongly localized within the molecule and that the required excitation energy be relatively low. Given these constraints, the classes of chemical compounds that are strongly fluorescent are few in number.

Aromatic hydrocarbons are, in general, intensely luminescent (4). The lowest lying electronic transition is often from a π-bonding orbital to a π^*-antibonding orbital. These transitions are characterized by high molar absorptivities ($\epsilon \geq 10^4$ M^{-1} cm^{-1}) (3). Aromatic hydrocarbons are resistant to bond dissociation due to the extensive delocalization of bonding electrons within the system of π orbitals.

The quantum efficiency for fluorescence is known to increase with increasing complexity of the aromatic system. This trend is accompanied by a shift toward longer emission wavelengths (4); thus the excitation of many aromatic hydrocarbons can be accomplished using light sources in the visible and near ultraviolet regions of the electromagnetic spectrum.

Apart from aromatic hydrocarbons, very few compounds are inherently fluorescent. These include some highly conjugated compounds such as ß-carotene and vitamin A and some aliphatic carbonyl compounds (3).

The chemical compounds that were selected for study by FFS are nonfluorescent. There are no conjugated π orbitals within any of the

compounds that were selected. For ammonia and the alkylamines, in particular, there are no π-bonding or nonbonding electrons. Furthermore, the energies associated with the absorption transitions are high, 180-160 nm in the case of acetonitrile (5) and from 250 to 160 nm for ammonia and the alkylamines (6). Photodecomposition, rather than fluorescence, is likely to occur in these compounds.

4. Methods that Extend the Applicability of Fluorescence Spectrometry

The reaction of nonluminescent analytes with fluorescent reagents to produce fluorescent derivatives is one way to expand the applicability of fluorometry. Fluorescence derivatization is usually carried out in order to increase the sensitivity of detecting the analyte (4).

Fluorescence derivatization techniques suffer from two fundamental disadvantages. First, fluorescence derivatization is not universal; different fluorescent derivatives must be used for different classes of chemical compounds. Second, derivatization reactions are not overly selective. Reaction products of the same chemical class will have the same absorption and emission spectra necessitating the use of chemical separation either before or after the reaction is carried out but before the fluorometric analysis is performed (1).

The indirect measurement of nonfluorescent compounds by the measurement of changes in background fluorescence has been reported. Several analytical applications have been developed to measure oxygen

based on collisional quenching of luminescence. A decrease in fluorescence or phosphorescence intensity due to the transfer of energy from the activated molecule to oxygen, the quencher species, has been related to partial pressure, diffusion rates, and permeability of oxygen (7). Another approach used in liquid chromatographic detection has been to monitor the change in background fluorescence of a fluorescent solvent (or solvent component) upon the elution of nonfluorescent analytes (8). These methods lack general applicability, however, as they tend to be restricted to the determination of a specific analyte, e.g., O_2, or to the use of a specific chromatographic solvent/analyte system.

In this dissertation, the study of an alternative approach to fluorometric measurements of nonfluorescent compounds is described. The technique is based on the conversion of the nonluminescent analyte into fluorescent fragments by using either electron impact (EI) or laser photolysis (LP). Fragmentation is carried out in the gas phase, at pressures ranging from 10^{-7} to 10^{-3} torr, to minimize the effects of bimolecular reactions (quenching) and chemical recombination (9). The approach, Fragmentation Fluorescence Spectrometry (FFS), takes advantage of the fact that many small molecular species and atoms fluoresce with high quantum efficiencies (10) and that virtually any molecule can undergo fragmentation provided enough energy is imparted to it in the form of energized particles or photons. Moreover, most molecular fragments have absorption and emission spectra that are in the easily accessible UV, visible, and near-IR regions of the

electromagnetic spectrum (11,12). Some examples of fluorescent fragments include OH, NH, CH, CN, HCO, SH, PO, CCl, CF, CO^+, and, C_2, and atomic fragments such as H, C, and most metal atoms. Fluorometric studies using the two different fragmentation techniques, electron impact and laser photolysis, will be discussed separately and thus will be referred to as either EI-FFS or LP-FFS.

B. Electron Impact-Fragmentation Fluorescence Spectrometry

1. Introduction and Theory

Fragmentation of gas-phase molecules is accomplished by electron-impact bombardment when electron energies in excess of 30 eV are used. In electron impact, electron energies of 70-150 eV are typical; however, the amount of energy actually deposited will depend upon the probability for the energy transfer to a given molecule which is, in turn, a function of electron energy (13). Probability curves are used to describe this process. The curves usually have a maximum absorption of electron energy at just above the ionization potential (IP) for the molecule (13). Fragmentation may occur directly to produce ions, excited ions, and excited neutral species (13). However, for a fraction of the electron-molecule collisions, an energy of less than the IP is transferred to the molecule to promote it to an excited state. The molecule may then dissociate to form fragments both in ground and excited states (13). Electron impact produces excited ions and neutrals of both fragment and parent species.

The measurement of an excitation function (fragment emission as a function of electron energy) for a particular fragment species yields the threshold energy (appearance potential) for the production of the fragment (14). This information can be helpful in understanding the fragmentation mechanism involved for molecular dissociation (15,16,17).

A plot of the fluorescence intensity of fragments versus photon wavelength at a given electron energy is called a fluorescence spectrum (14). This is completely analogous to fluorescence spectra that are optically-induced. Likewise, excitation spectra can be generated by electron impact by varying the electron energy while monitoring emission intensity at a particular wavelength.

2. Literature Review

a. Electron Impact of Ammonia, Aliphatic Amines, and Acetonitrile. The electron-impact induced fluorescence from the compounds ammonia, methylamine, and acetonitrile has been investigated by several workers. Using electron energies of 150 eV, Kuwata, et al. (18) detected fluorescence due to NH(A-X), CN(B-X), CH(A-X) and the Balmer series of atomic H lines from methylamine. The same fragments were produced by Fujita (19) from methylamine using electron energies of ~100 eV. Also, excited state NH radicals and atomic H were produced by the electron bombardment of ammonia; emission corresponding to the $A^3\pi$-$X^3\Sigma$ and $c^1\pi$-$a^1\Delta$ transitions of NH (15,17-25) and from H-Balmer transitions (15,17,21) were reported. The production of excited H (the

Balmer series) and CN(B) produced by the electron impact of acetonitrile has been reported by Tokue, et al. (26,27).

For these molecules, the appearance of the emission spectra tends to be independent of sample pressure and electron beam current over the same ranges employed in this study. The emission signals due to NH(A-X)0,0 and H_β transitions produced by EI of CH_3NH_2 were found to be linear with electron beam currents from 30-170 μA (18). In the same study, signal linearity was also exhibited for these fragment emissions over a range in sample pressures from 1-7 x 10^{-4} torr at 150 eV. These results imply that the excited species were produced by single electron-molecule collisions and that dissociation of the parent molecule was unimolecular. Similar results have been reported based on NH(A) and NH(c) produced from ammonia over ranges in electron currents and sample pressures of 10-50 μA and 2-8 x 10^{-5} torr, respectively (20).

Electron-impact studies of ammonia have been carried out to measure the appearance potentials of NH(A-X) and NH(c-a) (15,17,24), to measure the radiative lifetimes of NH($A^3\pi$) and NH($c^1\pi$) (20,22,23), and to study the mechanism of dissociative excitation (15,19,24). The absolute emission cross-sections of NH(c-a), NH(A-X), and H lines of the Balmer series were measured at incident electron energies of 100 eV (17). Similar studies of the formation of NH(A) and NH(c) produced by electron impact of ammonia and methylamine have been carried out by Kuwata (25) and Tokue (28). Emissive fragments produced from these compounds and from other alkylamines were studied by Johnson (21).

b. EI-FFS as a Method of Chemical Analysis. At this time there are few reports in the literature of work that utilizes optical detection of molecular fragments formed by EI as the basis for compound analysis. The first appearance of the concept used EI-FFS as the basis for a gas chromatographic detector (13). However, there were no detection limits, or studies of signal linearity or reproducibility reported. Some initial analytical figures of merit (limits of detection, linear dynamic range, and precision) for the compounds N_2 (29), CH_3NO_2, 1-nitropropane, 2-nitropropane, and CH_2Cl_2 (30) have been obtained by EI-FFS by this group. Studies of pressure dependence, electron energy dependence, threshold energy measurements, and excitation curve measurements have been made for ethanol, acetone, acetaldehyde, 1-propanol, and 2-propanol to assess the ability to differentiate between similar compounds based on their fragment fluorescence spectra (31).

C. Laser Photolytic-Fragmentation Fluorescence Spectrometry

1. Introduction and Theory

The use of laser radiation to accomplish fragmentation and/or ionization of gas-phase molecules is well established (32-34). Lasers offer distinct advantages over conventional, broad-band sources (32,35). The high spectral power densities of lasers may exceed those of conventional lamp sources by many orders of magnitude (35). This characteristic allows the spectroscopist to take advantage of nonlinear spectroscopic techniques (35) whereby the success of the experiment is

dependent upon the absorption by the molecule of more than one photon. Moreover, with the use of lasers the sensitivity of nonlinear techniques is enhanced since the production of high abundances of atoms and/or free radicals can be localized within very small volumes (32).

Extremely narrow spectral bandwidths are available with most lasers, e.g., $\Delta\nu$ = 0.03 cm^{-1} (32), permitting discrete rovibronic states to be accessed. This feature results in improved spectral resolution since resolution, typically limited by instrumental bandwidth, may be instead limited by the spectral linewidth of the absorbing or emitting molecules (35).

The high collimation of laser beams results in a significant reduction in scattered background radiation in the sample-beam interaction region (35). Low beam divergence allows one to more efficiently reduce scattered laser light. The coherent nature of lasers also enhances the efficiency with which any laser-induced luminescence can be detected; the dimensions of the interaction zone are typically so small that it can be efficiently imaged onto the entrance slit of a monochromator (35).

Laser-based techniques in multiphoton photolysis have become the standard method used to prepare free radicals for spectroscopic studies (33). Two types of multiphoton absorption processes are recognized. Those absorptions which occur through a non-stationary intermediate or a so-called "virtual state" are referred to as "simultaneous" absorption processes (33). The virtual state possesses a lifetime that is infinitesimally small (10^{-15} s); thus, simultaneous absorptions are

characterized by very low absorption cross-sections and can only be observed or detected when very intense laser fluxes (~10^{6} W/cm^2) are used (32). A second route of nonlinear excitation occurs when the energy of the incident photon is resonant with a real or stationary intermediate state (33). Such absorptions are referred to as "resonant" or "sequential" processes. Since resonant excitation occurs via intermediate states that are typically of longer lifetimes (10^{-6}-10^{-9} s), excitation through sequential, one-photon absorptions can be quite efficient.

In laser-induced fragmentation, the experimental basis for LP-FFS, sequential absorption processes are the preferred route to the production of molecular fragments for two fundamental reasons. Sequential absorption processes can be an efficient use of photons; the value for a photon-absorption cross-section mediated by a resonant state is much larger than for processes occurring via virtual states (33). Resonance-enhanced multiple photon ionization (REMPI) techniques have been used to achieve unit ionization efficiencies (32).

Since the sequential absorption of more than one photon occurs through a real intermediate state there exists the potential for the application of LP-FFS to the analysis of multi-component samples. The potential exists to selectively photolyze individual constituents of a mixture based on the differences in their absorption spectra. This experimental capability has already been demonstrated for REMPI (32,36,37).

Due to the stepwise nature of nonlinear photochemistry, excited molecules may fragment and/or ionize depending on the relative rates for the pathways involved for each. In general, the lifetime of a virtual state is too short for molecular dissociation to occur; thus, photochemical transformations typically have as their origin the first excited resonant state (34). The various processes proceeding from the resonant state have been categorized by Gedanken, Robin, and Kuebler into three different classes (34). A compound will exhibit "class A" or "class B" behavior depending on what happens at the resonant state; the molecule may absorb one or more photons and ionize or bond dissociation may occur before another photon can be absorbed (34).

In "class A" systems the parent ion is formed when the rate of photon absorption to excite the molecule into the ionization continuum is greater than the decomposition rate from any accessible resonant state (34). Once produced, the molecular ion is available to undergo subsequent excitation to produce both neutral and ionic fragment species, For class A systems, the general course of events is ionization followed by fragmentation (34).

Class B systems are characterized by large dissociative relaxation rates from one or more resonant states. There is a greater probability that the excited molecule will fragment before another photon can be absorbed (34). As for class A systems, the fragments produced by a class B mechanism may continue to absorb photons via resonant states and fragment until only atoms remain (34).

Whether a molecule can be classified as either a class A or class B system will depend upon the relative rates of dissociation and absorption in the molecular resonance state (34). Class A molecules tend to be multiply-bonded organics of low-molecular-weight atoms, while class B systems consist of inorganic and organometallic compounds (34).

The third case, known as "class C", includes those fragments that are postulated to be produced by the dissociation of a parent molecule in a super-excited state. Such a state can be produced by the simultaneous absorption of many photons to excite the molecule into its ionization continuum. The super-excited parent then dissociates, a process referred to as the "big bang," to yield fragment ions, neutrals and atoms (34). Authenticated cases of "class C" behavior are few in number.

2. Literature Review

a. Laser Photolysis of Ammonia, Aliphatic Amines, and Acetonitrile

The mechanism for the photodissociation of ammonia to produce $NH(A^3\pi)$ has been well studied. Donnelly and coworkers were the first to observe the intense $NH(A^3\pi\text{-}X^3\Sigma)$ emission from the photolysis of NH_3 using an ArF excimer laser (38). The production of the excited imidogen radicals was initially attributed to a two-photon resonance process (38).

It is known that 193-nm photons are resonant with the first absorption band of ammonia ($170 < \lambda < 218$nm) (39). The excited

electronic state is a planar $\tilde{A}\ A''_2$ state of D_{3h} symmetry as opposed to the pyramidal $\tilde{X}\ A_1$ ground state (in C_{3v} symmetry). The upper state is believed to be strongly predissociative (38,40).

Upon the absorption of the first photon, NH_2 is thought to be formed by the rapid dissociation of $NH_3(\tilde{A}\ A_2)$. The absorption coefficient (ϵ) for the first step, based on the absorption spectrum of NH_3, was estimated to be 300 $cm^{-1}atm^{-1}$, indicating a large photolysis rate for that system (33% of NH_3 is destroyed by photolysis) (41).

The formation of excited $NH_2(\tilde{A}^2A_1)$ is likely to occur via a single-photon process (the dependence of $NH_2(\tilde{A}^2A_1\text{-}\tilde{X}^2B_1)$ fluorescence on excimer laser power has been shown to be linear (38)). Even though this does not confirm $NH_2(\tilde{A}^2A_1)$ as the precursor to $NH(A^3\pi)$, a single photon dissociation of NH_3 followed by secondary photolysis of the NH_2 photofragment was proposed (38).

There are further studies in support of this mechanism, power dependence studies show that for "modest laser intensities" the dependence of NH(A-X) fluorescence on ArF excimer laser intensity is nearly quadratic (n = 1.9) (41), and that $NH_2(\tilde{A}^2A_1)$ can absorb the second 193-nm photon to produce $NH_2(\tilde{B}^2B_2)$ which then dissociates to produce $NH(A^3\pi)$ (42). Evidence that the excited state of NH_2 serving as the major precursor to $NH(A^3\pi)$ may be other than the $\tilde{A}^2A_1$ state is given by an estimated quantum yield for the production of this species by the first photon absorption of only 2.5% (38,43).

The use of two 193-nm excimer lasers was successful in providing further experimental grounds for the assignment of the intermediate

species as excited NH_2; however, the authors were not able to clarify the identity of the excited electronic state ($\tilde{A}^2A_1$ vs. $\tilde{X}^2B_1$) (44).

Lifetime measurements for $NH(A^3\pi\text{-}X^3\Sigma)$ fluorescence have been made by numerous workers (45,42,41,46). The production of $NH(a^1\Delta)$ by the 193-nm photolysis of ammonia has also been observed (39,40).

There exist in the literature instances in which NH radicals are formed and then laser-induced fluorescence (LIF) in the $A^3\pi\text{-}X^3\Sigma$ system is carried out. Fairchild, et al. (45) use a Nd:YAG-pumped dye laser, frequency-doubled, to excite NH through the (0,0) bandhead near 336 nm and the (1,0) bandhead near 305 nm, in order to excite single rotational levels and thus more accurately assess radiative lifetimes and relative transition probabilities for A-X (v' = 1 and 0). The radiation lifetimes of the v' = 1 and 0 levels were found to be 420 ± 35 and 440 ± 15 ns, respectively. A trace amount of NH_3 in a microwave discharge (1 torr total pressure) was used to generate NH(X).

In order to determine rate constants for quenching of NH(A), NH(X) was excited on the $R_1(7)$ transition at 333.1 nm while the A-X(0,0) band at 336 nm was monitored (47). Enhancement of NH(A-X) fluorescence by the use of an additional tunable-wavelength dye laser was reported. The NH radicals were produced by "laser pyrolysis" in a flow-through cell at 30 mtorr NH_3, 14 torr total pressure.

The photochemistry of methylamine has been investigated using excimer laser radiation at 193 nm (48,49). Fluorescence from the fragments NH, CN, and CH were observed in the wavelength range of 200-500 nm. The dependencies of fluorescence intensity for these fragments

on intensity of the photolysis laser energy are also reported (48,49). Nishi, et al. (48) found that the fluorescence intensity of CN varied as the second power of the energy of the photolysis laser (n = 2) and for the fragments NH and CH, they found n to equal 1.5 and 1.6, respectively. Values of n determined using an unfocused photolysis laser beam were slightly higher; n was found to be 2.4, 1.7, 1.8 for the fragments CN, NH, and CH, respectively (49). Fluorescence lifetimes are reported by Haak and Stuhl (49) for $NH(A^3\pi)$ and $CH(A^2\Delta)$. The fluorescence lifetime of $NH(A^3\pi, \nu' = 0)$ was determined to be 470 ± 30 ns, while that of $CH(A^2\Delta, \nu' = 0)$ was reported as 520 ± 50 ns.

Two excimer lasers have been used in "pump-probe" experiments to elucidate the nature of the photofragmentation mechanism for CH_3NH_2 (44). The NH(A) and CH(A) were found to behave similar to NH(A) formed from ammonia (44). Earlier results indicating that the absorption of at least 3 photons is necessary for the formation of CN(B) (49) were supported. Moreover, it was shown to be likely that two photons were responsible for forming an intermediate species and one further photon to excite the CN(B) (44).

Lee and Bischel (50) have measured ion currents produced by the two-photon ionization of methylamine in order to determine the associated ionization coefficients. The ion current was found to be proportional to the square of the laser intensity; the two-photon ionization coefficient (α) for methylamine was found to be 6.8×10^{-28} cm^4/W and the photoabsorption cross-section (σ) to be equal to 1.9×10^{-18} cm^2.

Currently, there are no reports in the literature that demonstrate the production of fluorescent fragments by the photolysis of acetonitrile using an ArF excimer laser. This is consistent with what is known of the UV absorption characteristics of that molecule. Acetonitrile has two continuous absorption systems, from 180-160 nm and from 160-130 nm (5). Laser photolytic studies of acetonitrile consist of the use of the fourth harmonic of a Nd:YAG laser at 266 nm of 25 ps pulsewidths (51,52). Fluorescence from CN($B^2\Sigma$) emission was observed and the fluorescence decay curve indicated the presence of more than one mechanism for the production of CN(B). The process required the sequential absorption of at least 2 photons (51).

The cyanogen radical has been investigated by numerous workers using "photolysis-probe" laser-based techniques. Excitation LIF spectra are used to study state population distributions of CN($X^2\Sigma$); parent molecules: fumaronitrile (53); BrCN (54); ICN (55). Excitation LIF of CN(X) radicals produced by the laser photolysis of NCNO have been used in determining the dissociation dynamics for the process (56,57). Vacuum UV-flash lamp photolysis of C_2N_2 followed by LIF of CN(X) was used to determine fluorescence lifetimes for individual rotational states of CN(B-X) (58). The radiative lifetime of the "unperturbed rotational levels" was found to be 65.6 ± 1.0 ns. Kawazumi and Ogawa (59) used LIF to measure the rotational temperature of ground-state CN fragments produced by the electron-impact induced dissociation of CH_3CN. Rotational state populations were also determined using LIF of CN fragments produced by electron impact (60).

b. Applications of LP-FFS. Examples of laser-induced photofragmentation, with subsequent measurement of fragment emission, as applied to the quantitative analysis of compounds, exist in the literature. A detection scheme based on NH(A-X) fluorescence produced by the photolysis of ammonia using 193-nm excimer laser radiation was used to determine ammonia above solutions of ammonia in water (61). The authors used their results to demonstrate the feasibility of remote detection of atmospheric pollutants. In situ analyses of PH_3 and AsH_3 based on the fluorescence of PH_2 and AsH_2 have been carried out in chemical vapor deposition reactors (62). As another application of FFS to remote detection, the salts, NaCl and KCl, have been determined in combustion cells using the emission from Na and K, respectively. Part per billion sensitivities and linear dynamic ranges of 3 to 4 decades were reported (63). Dimethyl methyl phosphonate has been studied for the production of PO fluorescence in a 2-laser, "photolysis-probe" experiment. The work is proposed as a detection scheme for organophosphonates (64). Limits of detection, linear dynamic range and precision are reported for the determination of CH_3NO_2 based on CH emission (65). Also reported are the detection of methanol, acetone, and various alkanes (fragment: CH) (66); aliphatic amines (fragment: CN) (30); and volatile metal chelates (fragment: the metal atom) (67). And finally, the feasibility to detect atmospheric HNO_3 has been recently discussed using $OH(A^2\Sigma)$ emission (68).

D. Objectives of This Research

The primary objective of this research was further to investigate the analytical utility of EI-FFS and LP-FFS. Several nonfluorescent compounds have already been analyzed using FFS; the limits of detection, linear dynamic range, and analytical precision have been determined for N_2 (29), nitro-compounds, and halogenated alkanes (30) by EI-FFS and nitromethane (65) and volatile metal chelates (67) by LP-FFS.

Contained in this work are the results of the analysis of a small group of compounds by both EI- and LP-FFS. These results are used to compare the two techniques on the basis of analytical sensitivity, linearity, and reproducibility.

Given that the basis of FFS lies in the ability to form molecular fragments and/or atoms that are electronically excited, it is important to investigate any effect that increasing molecular complexity may have on the sensitivity of the technique. A group of chemically similar compounds having a range of molecular weights were analyzed by LP-FFS. The results of these studies are used to discuss LP-FFS in terms of this so-called "heavy molecule effect."

If one assumes that any fragment or atom is produced with efficiencies of less than 100% then the opportunity exists to improve the sensitivity of FFS by inducing additional fluorescence from those fragments or atoms initially formed in the ground electronic state. Initial studies in this laboratory involving this approach have proved successful for the analysis of a volatile copper chelate by LP-FFS in

which a second, tunable-wavelength, pulsed dye laser was used to excite a particular electronic transition of the bare copper atom (67). In the work that is presented here, a second laser in conjunction with LP-FFS was used in an attempt to improve the limits of detection for three molecular fragments.

CHAPTER II

EXPERIMENTAL

A. Introduction

This chapter consists of three major divisions, one each devoted to EI-FFS and LP-FFS and the third dealing with the use of a probe laser in LP-FFS. Each division is further subdivided into two sections. Each first section describes the instruments that are used to carry out the experiments. Separate instruments were used in the electron-impact and laser-photolytic experiments. The second section for each division describes the experimental procedures pertaining to the use of each instrument and the collection of data. A list of the compounds analyzed, according to each technique, is given in Table 1.

B. Electron Impact-Fragmentation Fluorescence Spectrometry

1. Instrumentation

a. Fragmentation-Fluorescence Spectrometer. A block diagram of the electron-impact fragmentation fluorescence spectrometer is given in Figure 2. The vacuum system is shown in Figures 3 and 4 and consists of a custom vacuum chamber (MDC Manufacturing, Hayward, CA) made of 304 stainless steel with a volume of approximately 8 L. Conventional 10-cm diameter vacuum tubing forms a cross of about 33 x 51-cm dimensions. An additional 15.2-cm length of 10-cm diameter tubing is attached to the longer dimension. There are 4 ports, each approximately 7.6 cm in

Table 1. Compounds analyzed by EI- and LP-FFS.*

Compound	Structural Formula	EI-FFS	LP-FFS
ammonia	NH_3	x	x
methylamine	CH_3NH_2	x	x
acetonitrile	CH_3CN	x	x
n-butylamine	$C_4H_9NH_2$	-	x
diethylamine	$(C_2H_5)_2NH$	-	x
n-hexylamine	$C_6H_{13}NH_2$	-	x
dibutylamine	$(C_4H_9)_2NH$	-	x
tributylamine	$(C_4H_9)_3N$	-	x
n-tetradecylamine	$C_{14}H_{29}NH_2$	-	x
n-hexadecylamine	$C_{16}H_{33}NH_2$	-	x

*X's denote compounds that were analyzed by a particular technique.

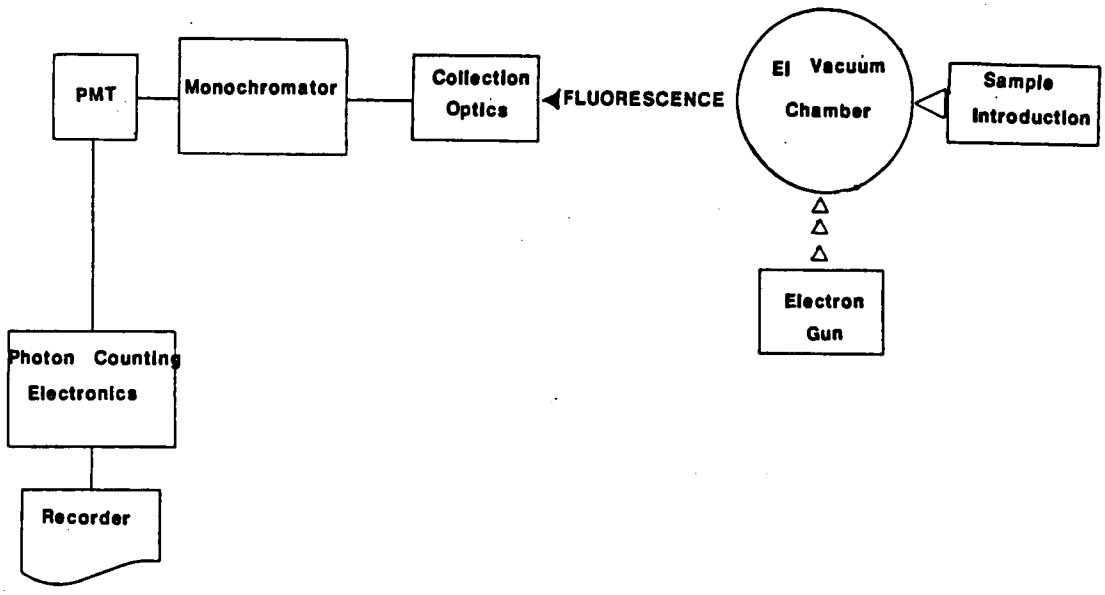

Figure 2. Block diagram of EI-FFS instrumentation.

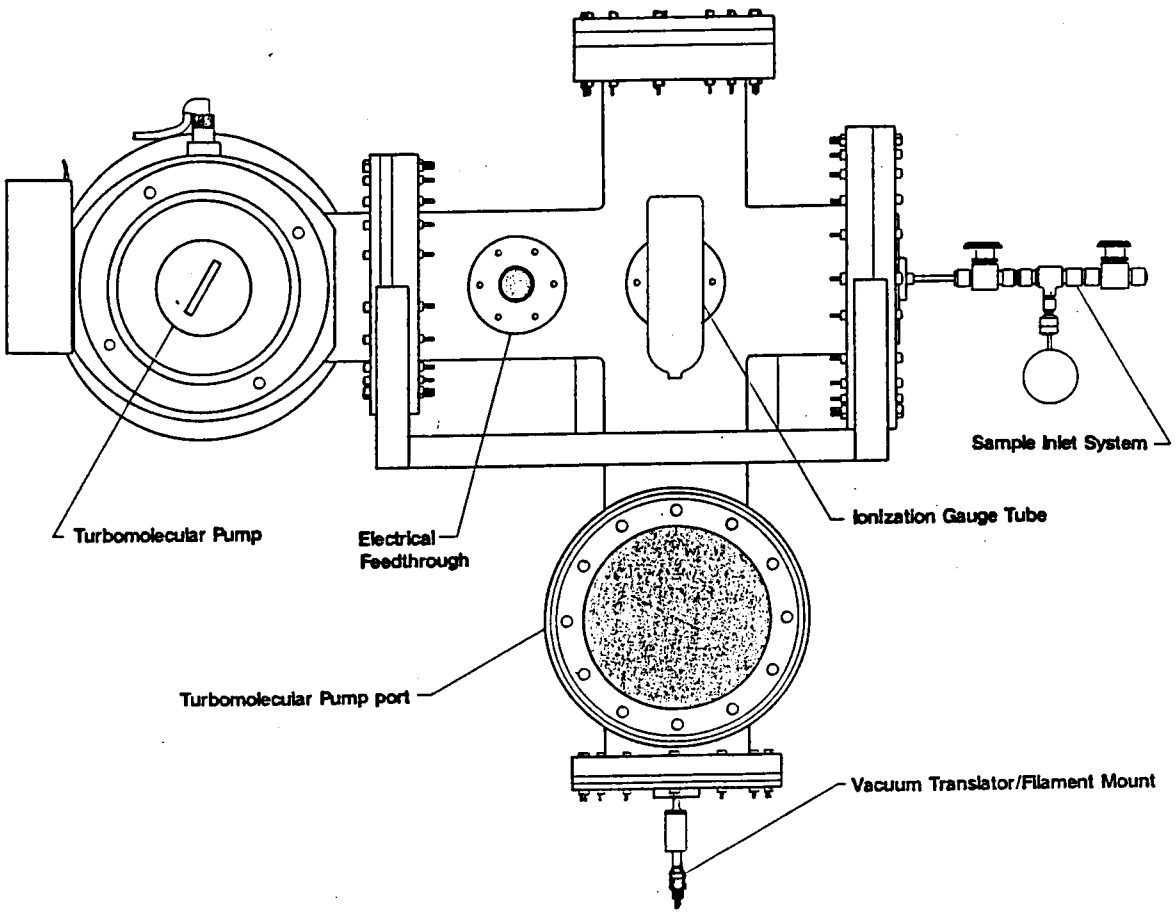

Figure 3. EI-FFS vacuum chamber--external view.

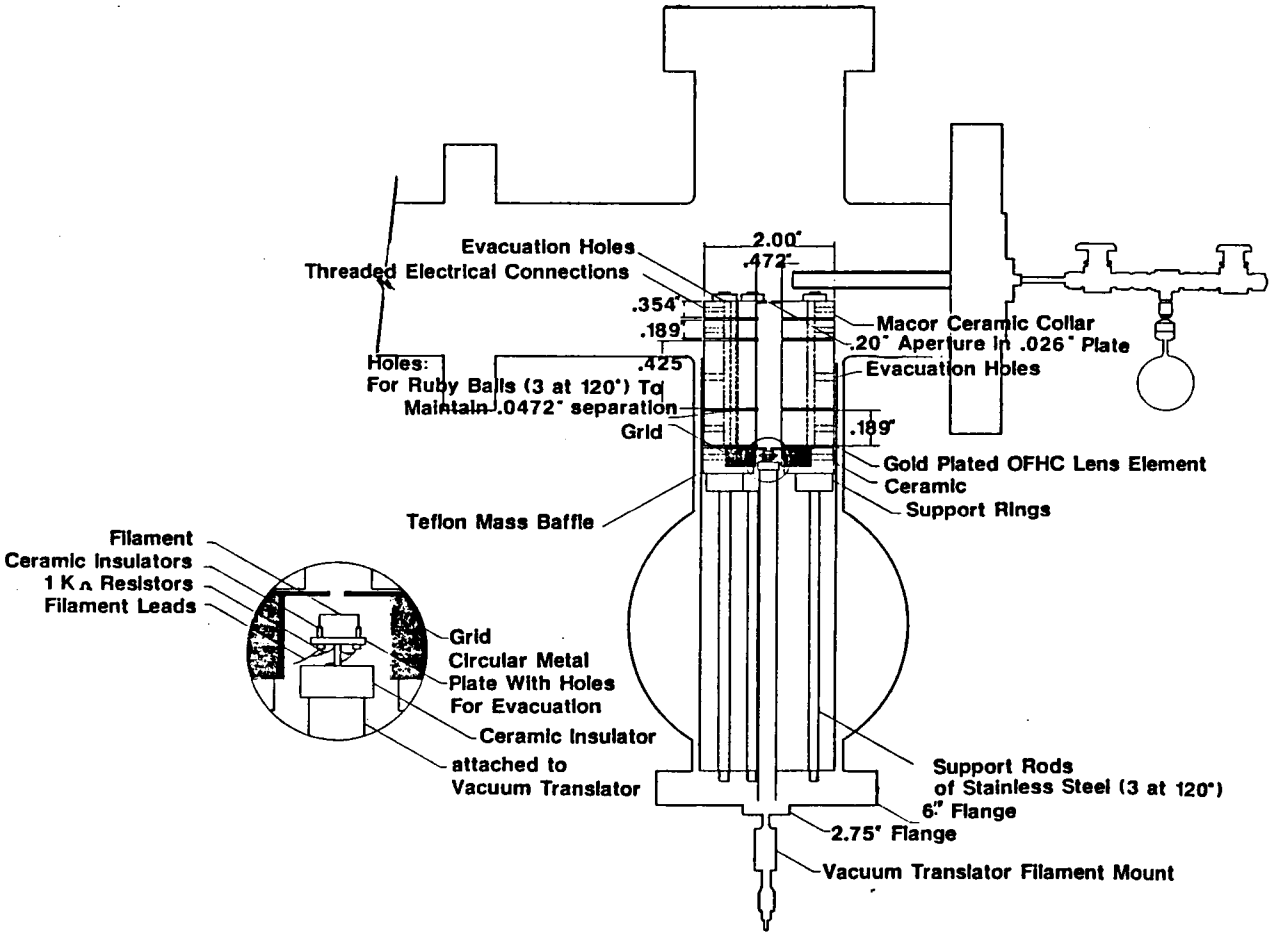

Figure 4. EI-FFS vacuum chamber--internal view, showing electron gun.

length, with 7-cm flanges attached via 3.8-cm diameter tubing. An additional port is attached with tubing and a 3.4-cm flange. A 6.1-cm diameter quartz vacuum viewport is attached by an 11.4-cm diameter flange at the center of the cross.

There are two compartments in the vacuum chamber, separated by the lens assembly of a homemade electron gun. A Teflon gasket press-fit between the walls of the chamber and the ceramic base which holds the electron gun is used to isolate the two chamber compartments. The only means of mass conductance between the compartments is via the 3 mm aperture of the grid, the first lens element encountered by the electron beam.

The chamber is differentially pumped with two turbomolecular pumps (Model TSU 331 pumping systems, Balzers Pfeiffer, Hudson, NH) with pumping speeds of 300 L/s for nitrogen, 330 L/s for hydrogen, and 370 L/s for helium.

The pressure in the vacuum chamber in the absence of sample was approximately 5-7 x 10^{-8} torr. In the presence of sample, pressures in the electron-sample interaction region were as large as 1 x 10^{-3} torr, with corresponding pressures of about 1-2 orders of magnitude less in the filament region of the vacuum chamber.

Pressures less than approximately 5 x 10^{-5} torr were measured using a Bayard-Alpert ionization gauge tube (Model IK-100, Huntington Laboratories,Inc., Mountain View, CA). A Veeco Instruments (Long Island, NY) Model RG-81 ionization gauge controller was used to control the tube. Pressures greater than approximately 5 x 10^{-5} torr were

measured with a capacitance manometer (Vacuum General, San Diego, CA, Model CMH-01s03, 1 torr head, 80-6A control/display unit). A detailed description of the EI-vacuum system is given by Guilbault (69).

The sample introduction line was interfaced to the high-vacuum electron-impact chamber via a 1/4-inch stainless steel tube welded to the outer surface of a stainless steel plate, which was attached to the chamber at a 10.1-cm flange. On the high-vacuum side of the interface plate, a length of 1.6-mm outer diameter glass-lined tubing (0.7-mm inner diameter) (Scientific Glass Engineering, Austin, TX) was used to transfer sample to the electron-sample interaction region. The glass-lined tube could be resistively heated in order to prevent its clogging due to condensation of sample vapor. The glass-lined tube was positioned at 90° to and terminated at the electron beam. The electron gun was constructed according to the design of Erdman and Zipf (70). A diagram of the assembled electron gun is shown in Figure 4. Gold-plated electron lens elements separated by ruby spheres were used to electrostatically focus the electron beam into the electron-sample interaction region of the vacuum chamber. The filament material used was thoria-coated iridium (Troyonics, Kenvil, NJ) unless otherwise noted. Filaments were mounted on a vacuum translator (Model VF-109, Huntington Mechanical Laboratories) to permit adjustment and optimization of the filament-to-grid distance. A more detailed description of the electron gun is given by Guilbault (69).

The optics used for the collection of fluorescence were mounted on an optical rail positioned between the electron-impact apparatus and

the emission monochromator, as shown in Figure 2, allowing fragment fluorescence to be collected at right angles both with respect to the electron beam and to the sample introduction axis. A 15-cm focal length plano-convex fused silica lens was used to collimate the fluorescence which was then focused onto the entrance slit of a 0.25-m grating monochromator (Kratos, GM-252) by a 20-cm focal length plano-convex fused silica lens. The lenses were manufactured by ESCO Products (Oak Ridge, NJ).

Current pulses from a photomultiplier tube (Model 8850, RCA, Harrison, NJ) were processed by photon counting equipment manufactured by EG&G ORTEC (Oak Ridge, TN). The photomultiplier tube (PMT) was housed in a Model 9201 PMT base connected to a Model 456 High Voltage Power Supply. The PMT was operated at +1750 V and the PMT output was the positive voltage taken from the 12th dynode. A Model 9302 Amplifier-Discriminator was routinely operated at high gain (x200 setting; 5 mV maximum amplitude range). The discriminator level was set by optimizing the signal-to-noise ratio of an emission signal as the discriminator level was varied. The amplified pulses were output to a Model 9315 photon counter. The photon counter dwell time was maintained at 1 s, enabling the counter to complete 15 cycles for each nanometer scanned by the emission monochromator. Typical dark count values were between 40 and 60 counts per second (cps). Digital-to-analog conversion was accomplished using a Model 9325 D/A converter. The converted PMT signal was output to an X-Y recorder (Omnigraphic 2000, Houston Instruments, Austin, TX) in order to obtain spectra.

The emission signal was measured as photon counts per second for each quantitative experiment.

b. Instrumental Optimization. Nitrogen was used to optimize the electron gun following each filament change. The fluorescence signal due to N_2^+ ($B^2\Sigma^+$-$X^2\Sigma^+$) at 391.4 nm was monitored for maximum intensity as the filament and grid potentials and filament-to-grid distance were varied. N_2^+ emission is very intense even at relatively low (ca. 1 x 10^{-5} torr) N_2 pressures. This aspect, along with the nonreactive nature of N_2 with respect to the filament material, makes it a good choice for optimization purposes. Typical values of optimal filament and grid potentials of -100V and -70V, respectively, were found to be in good agreement with those specified by Erdman and Zipf (70). By operating at a filament current of 3-4 A DC and 100 eV nominal electron energy, beam currents on the order of 1 mA (6 x 10^{15} electrons/s) were produced. The electron gun filament and grid potentials were optimized both before and after the positions of the fluorescence collection lenses were optimized.

A typical lens optimization procedure consisted of first removing the 20-cm f.l. lens and adjusting the remaining 15-cm f.l. plano-convex lens along the optical axis. The focusing lens was then translated at right angles to the optical axis and in and out of the vertical plane using a built-in pitch and yaw adjustment. The 20-cm f.l. plano-convex lens was then replaced to its position on the rail and adjusted along the optical axis. The same vertical plane and pitch and yaw adjustments were carried out as for the first lens. Finally, the

focusing lens axial position was finely adjusted using a translating device built into the lens mount.

c. Sample Introduction. The equipment used to introduce samples to both the electron-impact and laser-photolysis vacuum chambers consisted of the same design and materials. Sample transfer lines were constructed from 1/4-inch stainless steel tubing, the length of which depended on whether the sample was a gas or a liquid. For liquid samples the length of the tubing was no more than that needed to make connections on both ends using compression fittings (approximately 3 cm). For gases, much longer transfer lines (ca. 15 cm) were necessitated by the bulk and weight of the gas cylinders as well as by the need to safely secure the cylinders. Stainless steel compression fittings of 1/4-inch i.d. (Swagelok, Crawford Fitting Co., Solon, OH) were used in the construction of sample transfer lines.

The sample transfer line was connected to one end of a 1/4-inch Swagelok stainless steel tee. The other straight end of the tee was connected to the interface plate of the vacuum chamber via a stainless steel metering valve (Model 1315G4Y, Hoke, Cresskill, NJ or Nupro S-series, Willoughby, OH). For metering valves without the ability to form a high-vacuum seal when fully closed, e.g., the Nupro valve, a shut-off valve (Model CPI D4K-SS diaphragm-type, Parker Hannifin Corp., Huntsville, AL) was plumbed into the high-vacuum side of the metering valve. Sample pressure within both vacuum chambers was controlled by the use of the metering valve. The positions of the metering valve and the shut-off valve were as close as possible to the vacuum chamber.

This was done in order to facilitate pressure control by minimizing dead volume on the high-vacuum side of the metering valve.

The right-angled end of the tee was connected to an auxiliary glass vacuum line via 1/4-inch stainless steel tubing and a shut-off valve. This configuration permitted the sample introduction line to be evacuated prior to being opened to the turbomolecular pumping systems.

The gas cylinders were fitted with a high-purity, corrosive gas regulator (Air Products, Allentown, PA). Vapor from liquid samples was introduced into either the electron-impact or laser-photolysis chamber after each liquid sample had been thoroughly degassed through several freeze-thaw cycles. A reservoir of each liquid sample was provided by a glass bulb connected to the body of a glass valve made by Fischer Porter and Co. (Warminster, PA) having a Teflon valve-stem and O-ring seat and seals. Connected to the other side of this valve was a short length of 1/4-inch glass tubing which was used to attach the glass bulb/valve assembly to a sample introduction line via a 1/4-inch stainless steel O-ring-type adaptor (Cajon Ultra-torr, Cajon Co., Macedonia, OH). The O-ring material used in the handling of the samples was the elastomer ethylene propylene (Parker Seals, Lexington, KY).

Each time a vacuum seal through a compression fitting was broken or remade, the sample introduction line was tested for leaks in the following manner. The line, rough-pumped to a pressure of ca. 5 mtorr, was first opened to high vacuum while the pressure of the vacuum chamber was monitored. A rapid increase in pressure usually indicated

the presence of a leak. Any leaks from atmosphere could usually be confirmed by spraying the fitting(s) with small amounts of Freon while watching for transient deflections of the ionization gauge meter. First, the leaking compression fitting was tightened further. If, by subsequent testing with Freon, the leak persisted, the entire ferrule and tubing assembly was replaced with fresh ferrules and a clean tube terminus of uniform shape.

A slow, gradual increase in pressure to a value not exceeding ca. 1×10^{-6} torr was consistent with a properly sealed line. If this type of behavior was seen, the line was allowed to pump down overnight through the turbomolecular pumping system or until an acceptable base pressure had once again been attained. For the EI system, the chamber/line system was considered leak-free if base pressures in the upper compartment of the chamber (the sample-electron interaction region) were of the order of $1\text{-}3 \times 10^{-7}$ torr and the base pressures in the lower compartment (the filament region) were from $5\text{-}8 \times 10^{-8}$ torr. For the LP system, acceptable base pressures in the chamber/line system were $7\text{-}12 \times 10^{-8}$ torr.

The higher molecular weight compounds (those having vapor pressures of < ca.100 torr at 25° C) were heated with a heating mantle in order to increase their volatility. The sample introduction line was wrapped in heating tape and insulated in glass wool to maintain a temperature of at least 10° greater than that of the sample bulb to prevent the condensation of sample vapor in the line.

d. Samples. The gaseous samples, ammonia (99.99% anhydrous, Scott Specialty Gases, Plumsteadville, PA), and methylamine (98% anhydrous, MG Industries, Valley Forge, PA) were used without further purification. The following compounds were purchased from Aldrich Chemical Co.,Inc., (Milwaukee, WI) and used as received: acetonitrile, n-butylamine, dibutylamine, and tributylamine (99+% Gold Label); hexylamine (99%), and diethylamine (98%). Tetradecylamine (92%) was purified by vacuum distillation (150° C at 7 mtorr) just prior to analysis. Hexadecylamine (75%) was purified by vacuum sublimation (50° C at 7 mtorr) prior to analysis.

2. Experimental Procedures

a. Introduction. Following the acquisition of a survey spectrum for each sample, optimization of the filament and grid potentials of the electron gun as well as the positions of the collection lenses was performed in order to maximize the detection of the most intensely fluorescent fragment. However, if the same fragment was used for successive quantitative experiments for more than one compound, the reoptimization procedure was not repeated; therefore very similar experimental conditions were maintained from compound to compound.

This procedure was followed except in the event of a filament failure. Owing to the corrosive nature of the compounds analyzed, the filament had to be periodically replaced. Following the replacement of a filament, the electron gun was first optimized using N_2 as previously described (p. 32). This set of optimal experimental parameters was

usually checked upon reintroducing sample to the vacuum system. Again, only the most intensely emissive fragment was used for this purpose.

b. Emission Spectra. Electron impact fragmentation fluorescence spectra were acquired for each of the compounds listed in Table 1, page 25. The spectra were run in order to ascertain the identities of the fragment emissions produced by EI as well as their relative emission intensities. Typically, the emission monochromator was scanned over an approximately 200 nm range, in the region of ca. 300-500 nm. The monochromator slit widths were 250 μm, corresponding to a spectral bandpass of 0.83 nm. The remaining experimental parameters are given in Table 2. The most intense emission yielded by the survey spectum of a compound was used in subsequent quantitative experiments involving that compound.

c. Limits of Detection. The limit of detection (LOD) for any given sample was obtained using the following procedure. Sample was admitted to the vacuum system at a relatively low pressure (ca. 1 x 10^{-6} torr). The entrance and exit slits of the monochromator were adjusted to a predetermined width of 750 μm (bandpass = 2.5 nm) for maximal signal-to-noise ratio (S/N). The fragment emission was scanned over a spectral range that was wide enough to include a return of the recorder pen to baseline both before and after the emission peak if possible. This was done in order to establish a baseline for the spectrum. No instances arose wherein emissive features were so broad

Table 2. Typical values for experimental parameters used in EI-FFS.

Parameters	Experiments			
	Emission Spectrum	LOD	LDR	Precision
Filament current (A)	3.8	3.8	3.8	3.8
Filament potential (V)	-80	-100	-100	-100
Grid potential (V)	-50	-70	-70	-70
Sample pressure (torr)	$1x10^{-4}$	*	*	$2x10^{-6}$
Monochromator slit widths (μm)	150	750	350	700
Monochromator scan rate (nm/min)	4	4	4	4
D/A conversion range (cps)	10^1-10^3	10^0-10^2	*	10^1-10^3
Recorder amplification (mV/in)	500	500	*	200

*Variable

that they prevented the acquisition of a baseline on at least one side of the peak of interest within a scan width of approximately 10 nm.

A blank spectrum was acquired at the base pressure of the vacuum system under conditions identical to those used to obtain the emission spectrum. The blank spectrum was used to estimate the noise magnitude, N, which was subtracted from subsequent measurements of signal to provide a corrected estimate of signal magnitude, S. To measure the emission signal intensity, a baseline was drawn at a distance of 1/2 N above the lowest excursion made by the recorder pen during the scan. Signal magnitude was measured as the distance from the baseline to the maximum excursion of the recorder pen.

After the S/N was calculated, the sample pressure was adjusted and another emission spectrum obtained. The S/N was calculated and the procedure was repeated until a S/N of approximately 2 was obtained.

d. Precision. The reproducibility of the fluorescence was estimated by taking 12-14 replicate spectral scans of the emission peak while the sample pressure and all other experimental parameters were held constant. The sample pressure was set to a value of at least ten times that of the LOD for the corresponding compound. The number of replicate measurements, n, acquired was limited by either the time available before the sample pressure ceased to remain constant or n became equal to 14, whichever came first. At these signal intensities, the estimation of a spectral baseline was straightforward. The

experimental mean and standard deviation were computed and used in the calculation of relative standard deviation (RSD).

e. Linear Dynamic Range. Studies of the linear dynamic range (LDR) of the emission signal were carried out in the following manner. In general, initial measurements were made at sample pressures that yielded a S/N of approximately 2 under the chosen experimental conditions. The measurements were repeated for each incremental increase in sample pressure. Typically, 3 or 4 data points were acquired per decade in sample pressure. The D/A converter range and the recorder Y-scale attenuation were adjusted in order to keep the emission signal on-scale for each spectral scan. All other experimental parameters were held constant throughout the study. As for the previous two experiments, the wavelength scan range of the monochromator was such that a return to baseline on either one or both sides of the emission peak by the recorder pen was made. The width of each scan was sufficient to allow the magnitude of the baseline noise to be estimated for each attenuation setting of the X-Y recorder. For lower recorder Y-scale attenuation settings, an attempt to correct for baseline noise was carried out by drawing a baseline at one-half the magnitude of the baseline noise for each scan. The emission signal was measured as the distance from the baseline to the maximum excursion made by the recorder pen.

A summary of the experimental conditions used in acquiring the quantitative data is given by Table 2.

f. Pressure Measurement. The pressure readings obtained using the ionization gauge (IG) were usually corrected vis-a-vis the capacitance manometer (CM) pressure reading. The CM pressure readings are considered to be more accurate than those of the IG because the response of the former is independent of compound molecular weight. The correction was accomplished by calibrating the two pressure gauges in the region of ca. 5×10^{-5}-1×10^{-3} torr for each sample. The procedure used to obtain calibration data consisted of first establishing a stable sample pressure as indicated by the IG. At this pressure, both the CM and IG pressure readings were recorded. The sample pressure was changed and the procedure was repeated. An equation for the calibration curve was obtained by linear regression and used for the pressure correction. More information concerning the principles of operation of the vacuum gauges and their calibration may be found in the dissertation of Guilbault (69).

C. Laser Photolytic-Fragmentation Spectrometry

1. Instrumentation

a. Fragmentation Fluorescence Spectrometer. A block diagram of the laser photolysis fragmentation fluorescence spectrometer is shown in Figure 5. Figure 6 depicts the LP-FFS vacuum chamber and pumping system and sample introduction system. The vacuum chamber is of approximately 2 L volume. The chamber was constructed of standard 4-inch stainless steel vacuum tubing (ca. 9 cm long) welded to a stainless steel compartment of 14 x 12.7 x 9-cm outer dimensions. The

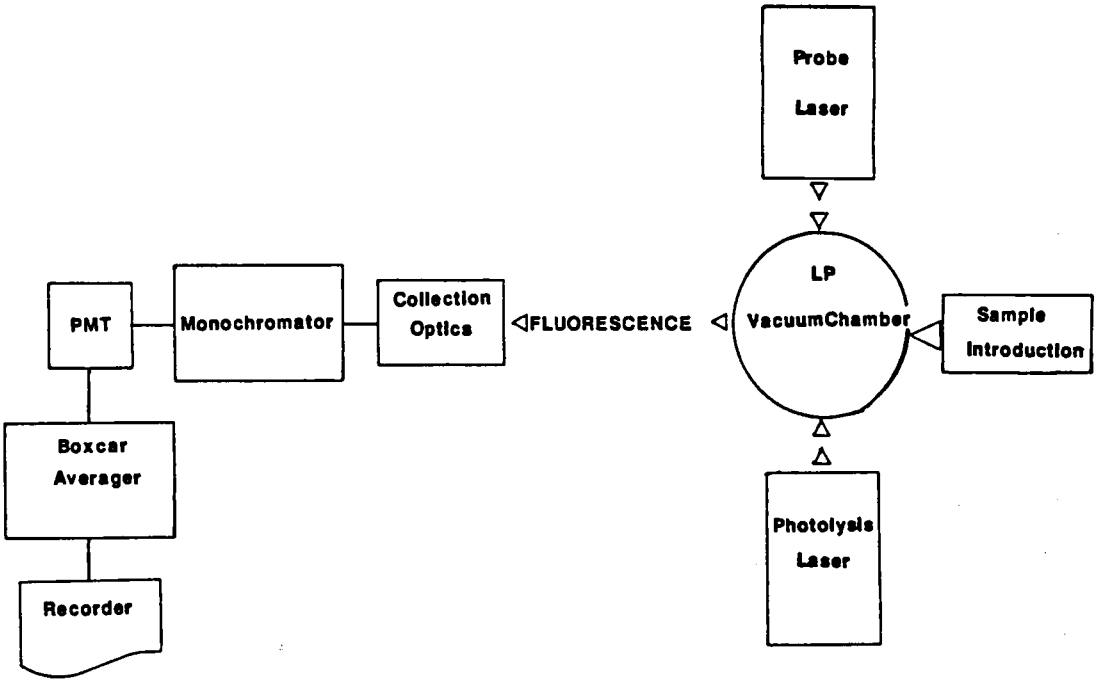

Figure 5. Block diagram of LP-FFS instrumentation.

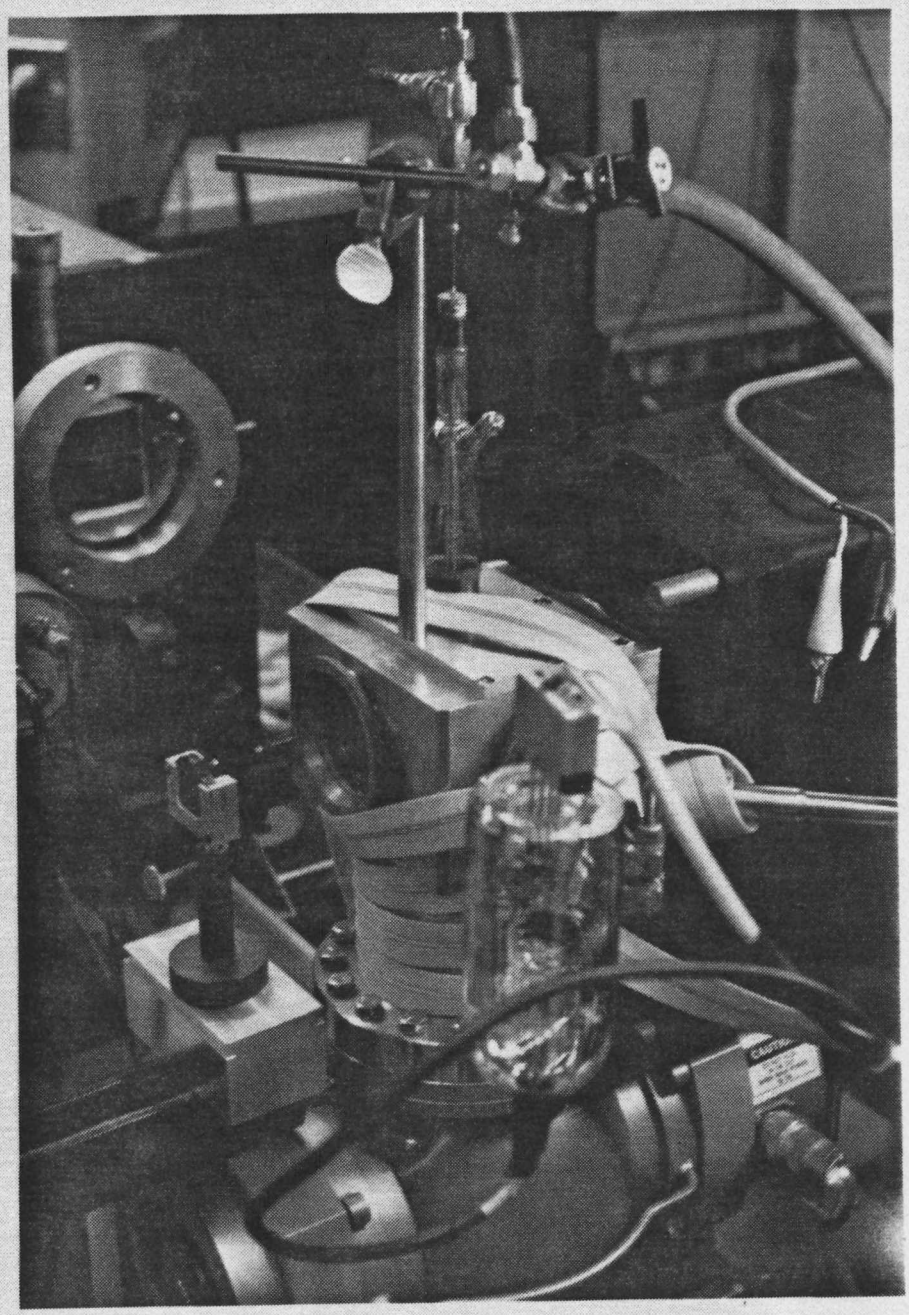

Figure 6. LP-FFS instrument showing pumping system, vacuum chamber, pressure measuring devices, and sample introduction system.

compartment contains 5 ports, 3 of which accommodate 6.4-cm fused silica windows or any 6.4-cm disc which can be sealed against atmosphere with O-rings. The fourth port was fitted with a custom-built, Y-shaped dual port of stainless steel tubing. Attached to the arms of the "Y" were a capacitance manometer and ionization gauge tube. These pressure measuring devices were identical to those used with the electron-impact instrument. Sample introduction apparatus could be attached at a fifth port located on top of the chamber. This port was rectangular (5.7 x 10.0 cm) and was designed to allow for flexibility in changes in sample introduction systems. An O-ring groove along the perimeter of this port provided an O-ring seal of a rectangular stainless steel plate (8.6 x 12.9 cm) against atmosphere. The plate could be either a blank piece of metal or one with an orifice through which sample could be introduced.

The chamber was pumped with a Balzers Pfeiffer turbomolecular pumping system (Model TSU 332) with pumping speeds of 300 L/s for nitrogen, 330 L/s for hydrogen and 370 L/s for helium. The vacuum system was attached to the chamber with a 6-inch Huntington "Vac-U-Flat" fitting. A more detailed description of the vacuum chamber design is given by Schendel (71).

The chamber pressure without sample was typically 5×10^{-8} torr; pressures as large as approximately 1×10^{-3} torr were observed in the presence of sample.

Samples were introduced to the chamber either as gases or vapor from pure liquids in a manner similar to the electron-impact

experiments. Two different systems of the same design as used by Schendel (71) were used to interface the sample transfer lines to the vacuum chamber. The first was constructed by welding a 0.5-mm inner diameter glass-lined tube (Scientific Glass Engineering) to the high vacuum side of an orifice in a rectangular stainless steel plate. The glass-lined tube terminated near the photolysis laser beam. Welded to the other side of the orifice was a 1/4-inch stainless steel tube to which the rest of the sample introduction system was connected.

For higher molecular weight compounds, it became necessary to heat the glass-lined sample introduction tube to prevent the condensation of vapor and clogging of the tube. A second sample/vacuum interface system similar to the first but capable of being heated in this manner was constructed using 0.75-mm inner diameter glass-lined tubing. The larger tubing size was chosen in order to further reduce the likelihood of clogging. The glass-lined tube was resistively heated. The tube was electrically insulated from the photolysis chamber at the rectangular plate and at the sample transfer line at its opposite end by being enveloped in a glass tube of ~2.7-cm outer diameter. Glass-to-metal connections were made using Kovar seals (Ace Glass, Vineland, NJ).

Fragments were generated in both excited and ground electronic states by laser photolysis at 193 nm using an ArF excimer laser (Model 2210, Questek, Billerica, MA). The laser repetition rate was always 10 pulses per second. The energy of the photolysis laser beam could be varied between approximately 40 and 120 mJ/pulse using on-board microprocessor control of the discharge voltage. See Schendel (71) for further operational details for the excimer laser.

The rectangular ArF laser beam was cropped to dimensions of 3.9 x 1.0-cm by an aperture before it passed through a 15-cm focal length plano-convex fused silica lens. The focused laser beam traveled a distance of approximately 13.5 cm before intersecting the sample at a position located approximately 0.5 to 1 mm below the sample introduction tube terminus.

Stainless steel baffles placed along the beam path 35 mm before and after its intersection with the sample vapor or gas allowed only the most intense part of the laser beam to pass through the sample-laser interaction region. The aperture dimensions in the baffles were 8 x 14 mm and 9 x 28 mm for the first and second baffles, respectively. The baffles served to minimize the extent to which reflected and scattered light, as well as fluorescence from the windows, entered the sample region of the chamber.

Fluorescence was collected at right angles to the photolysis beam and the sample introduction axis, collimated by a 12.7-cm focal length fused silica plano-convex lens, and focused onto the entrance slit of a 0.75-m grating monochromator (Model 1702, Spex, Metuchen, NJ) by a 15.2-cm f.l. fused silica cylindrical lens. The fused-silica plano-convex lens and cylindrical lens were manufactured by Oriel (Stratford, CT).

Signals from a photomultiplier tube (Model XP-2020, Amperex, Hicksville, L.I., NY) were taken to a gated integrator/ boxcar averager (Model SR-250, Stanford Research Systems, Palo Alto, CA) and then to an X-Y recorder (Omnigraphic 2000, Houston Instruments). The boxcar

averager was triggered by the signal from a UV photodiode (Model UV-040BQ, EG&G, Salem, MA) which was positioned in the path of the photolysis laser beam.

b. Instrumental Optimization. The preliminary photolysis laser beam alignment with respect to the vacuum chamber involved three separate components: the laser beam aperture, the UV photodiode, and the laser beam focusing lens. The laser beam aperture was positioned in front of the vacuum chamber along a rail. The aperture was placed as far from the laser output window as possible to minimize divergence of the beam. The aperture was centered on the beam so that only the most intense interior area of the beam was passed. The UV photodiode was clamped to a post attached to the same rail and positioned on the laser side of the beam aperture. The UV photodiode was oriented in the weakly intense beam periphery until a stable trigger of the boxcar averager was produced. The laser focusing lens was placed in a lens holder/mount assembly, positioned on the rail on the other side of the laser beam aperture and adjusted so that the laser beam was centered both vertically and horizontally on the 5-cm diameter lens. The lens was then moved in order to translate the focused laser beam either horizontally or vertically within the vacuum chamber to permit its alignment vis-a-vis the sample introduction tube. The alignment was accomplished by raising the focused beam high enough that, when moved back and forth, the beam could be seen as it interacted with the tube.

The optimal horizontal position of the lens was taken to be that which produced the most intense visible reaction of the tube to the

laser radiation. The focused laser beam was then lowered (by lowering the focusing lens) just until laser-induced light was no longer visible at the terminus of the tube. The position of the focusing lens along its optical axis was adjusted to a distance of approximately 13.5 cm from the sample introduction tube. At this distance the laser beam was slightly defocused at the point where it intersected the sample introduction axis.

The remainder of the preliminary optical alignment procedure consisted of alignment of the fluorescence collection lenses with respect to the monochromator. Sample was admitted to a pressure of ca. 1×10^{-4} torr and the laser output was set to a typical operating energy at 10 Hz pulse repetition rate. The plano-convex collection lens was placed on the optical rail at a distance of about 18 cm from the sample introduction tube. With the laboratory totally darkened, a faint bluish-violet image could be seen by placing a white business card between the lens and the monochromator. The collection lens was adjusted to cleanly position this image onto the entrance slit of the monochromator. At this point, the PMT power supply was turned on and the wavelength setting of the monochromator was adjusted to transmit radiation at a wavelength corresponding to the fragment of interest. The PMT output was sent via the boxcar unit to one channel of a dual-trace sampling oscilloscope (Model 7704A, vertical unit: 7A24, Tektronix, Beaverton, OR) and the boxcar gate to the other channel of the oscilloscope. The oscilloscope was externally triggered by the boxcar. The signal due to the boxcar gate was seen as a positive-going

signal at one channel of the oscilloscope and was distinguishable from the negative-going PMT signal observed at the other channel. The PMT signal was confirmed by opening the monochromator entrance slit cover while watching the oscilloscope display for a simultaneous negative-going shift in the baseline.

The signal was confirmed to be due to emission from the fragment of interest by observing the return of the PMT signal to baseline as the monochromator wavelength was scanned ± 3 nm from the nominal wavelength for fragment emission. A second check to confirm fragment emission was made by closing the sample valve and subsequently ruling out the possibility of any background signal at the same wavelength. As a final check, an estimate of the fluorescence lifetime was measured from the oscilloscope trace and its value compared to reported values in the literature. This also served as a preliminary confirmation of the identity of the fragment. A positive comparison between subsequent emission spectra and published spectra of the same fragment served as the final confirmation of fragment identity.

For final lens optimization, the boxcar-averaged signal was amplified and output to the X-Y recorder. The emission monochromator wavelength was manually optimized for maximum signal intensity as the monochromator slit widths were reduced. The slit widths were kept as narrow as possible (50-100 μm), while maintaining good signal-to-noise ratio, in order to increase the sensitivity of the signal output on changes in optical alignment. The position of the plano-convex collection lens, and then that of the laser focusing lens, was

optimized for maximal signal. The cylindrical collection lens was then placed onto the optical rail and its position was optimized. The positions of the two collection lenses were then adjusted alternately until the signal was maximized.

After confirming the production of fragment fluorescence induced by laser photolysis, it was necessary to establish certain experimental parameters before commencing with the LP-FFS experiments.

The boxcar averager was adjusted to be triggered at the minimum threshold voltage for maintaining a stable trigger. This procedure effectively minimized the inherent time delay between the triggering of the boxcar and the enabling of the sampling gate due to a nominal 20ns delay in the trigger discriminator.

The temporal width of the electronic gate of the boxcar averager was adjusted so as to maximize the signal intensity of each fluorescent fragment investigated. This procedure was typically carried out using a boxcar delay time (the time from the triggering of the boxcar by the laser pulse to the opening of the boxcar sampling gate) of 0 ns. For the NH fragment, a boxcar gate of 30 ns was found to produce the greatest signal; for the CN fragment, a gate setting of 10-20 ns was found to be optimal.

The optimal boxcar delay time was next determined by scanning the boxcar gate either manually or electronically (using the auxiliary gate scanner module (SR Model 200, Stanford Research Systems)) at a boxcar gate width of the optimal value determined previously. The range of the gate scan was generally of approximately the same magnitude as the

lifetime of the fluorescence being investigated. For the fragments NH (as produced from ammonia) and CN (as produced from methylamine) a signal maximum occurred at a delay time of 0 ns. Thus, a boxcar delay time of 0 ns was used in all subsequent experiments involving only the photolysis laser as it was desirable that the boxcar sample the most intense portion of the fluorescence decay curve. It should be recognized that the temporal resolution of these boxcar gate scans was limited by the width of the boxcar gate; thus, any changes in signal with boxcar delay time that may have occurred within the first 10-25 ns of the scan were obscured.

The emission due to NH ($A^3\pi$-$X^3\Sigma$) 0,0 and 1,1 transitions was used to evaluate the boxcar sampling rate. Based on the spectral resolution of the 0,0 and 1,1 transitions at 336.0 and 337.0 nm, respectively, a limiting criterion of a minimum sampling rate of 10 samples per average for every 0.1 nm scanned by the monochromator was established as being adequate for maintaining a good S/N. The boxcar averager experimental parameters are summarized in Table 3.

2. Experimental Procedures

a. Introduction. In general, fewer fragment emissions were observed in LP-FFS than in EI-FFS. For the analysis of the first two compounds, ammonia and methylamine, it was most expedient to assess the most intense fragment produced by each compound before collecting an emission spectrum. This was accomplished by scanning the monochromator through a 300-500 nm range by hand after the collection lenses had been

Table 3. Typical values for experimental parameters used in LP-FFS.

Parameters	Experiments				
	Emission Spectra	Power Dependence	LOD	LDR	Precision
Sample pressure (torr)	$1x10^{-4}$	$1x10^{-4}$	*	*	$2x10^{-5}$
Laser energy (mJ/pulse)	70	*	80	80	80
Monochromator slit widths (μm)	100	100	350	250	250
Monochromator scan rate (nm/min)	5	5	0.5	2	2
Boxcar gate (ns)	*	20	20	20	20
Boxcar gain (mV/V)	50	50	50	*	50
Boxcar samples/ave.	10	10	100	30	30
Recorder amplification (mV/in)	500	500	50	*	500

*Variable

properly positioned (see pp. 48-49). The final optimization of the optics and signal processing parameters were then performed with the monochromator tuned to transmit the most intense emission. For the analysis of each succeeding compound the fluorescence collection lenses were reoptimized only as needed and identical signal processing parameters were maintained within each type of experiment. A summary of the experimental parameters used in the LP-FFS experiments in given in Table 3.

Peak heights were measured in inches and normalized to volts for all of the quantitative LP-FFS experiments.

b. Emission Spectra. Following optimization of the LP-FFS instrumentation, emission spectra were obtained for each compound in the region of approximately 320-440 nm. The monochromator slit widths were typically 100 μm (spectral bandpass = 0.1 nm). The settings of the boxcar averager used to detect the fluorescence were established by the methods described in section II.C.1.b. (pp. 50-51) and were based on the most intense fragment emission. For ammonia, NH(A-X) fluorescence was the only fluorescence observed in the region from 300-500 nm and was quite intense. For each alkylamine the most intense fragment emission was due to $CN(B^2\Sigma\text{-}X^2\Sigma)$. The laser energy used was the maximum that provided stable operation at 10 Hz repetition rate (ca. 60-80 mJ/pulse) over the duration of the scan. Blank emission spectra were collected using identical experimental conditions.

c. Power Dependence Studies. In order to determine the optimal laser energy to be used in quantitative experiments, the power dependence of fragment fluorescence intensity on laser energy was investigated. The procedure consisted of admitting sample to the vacuum chamber at a relatively high pressure (ca. 1×10^{-4} torr) so as to enhance S/N. While the sample remained at constant pressure, the spectral feature of interest was scanned at various photolysis laser output energies. Usually, 4 scans were acquired for each laser energy setting. A log-log plot of average emission intensity vs. the average value for per-pulse laser energy yielded the power dependence as the slope of the line. For subsequent experiments, the laser energy was chosen such that the power dependence of fragment fluorescence was minimized while maintaining stable laser operation.

d. Limits of Detection. Certain experimental conditions used in obtaining the limit of detection for each fragment were established using the NH(A-X) fluorescence produced by ammonia. The optimal values for the slit widths of the monochromator and sampling rate of the boxcar averager were determined by alternately holding one constant while the other was varied until no further increase in S/N could be obtained. The slit widths of the monochromator and boxcar sampling rate found to be optimal for this experiment were 350 μm, corresponding to a spectral bandpass of 0.35 nm, and 100 samples per average, respectively. The remaining experimental parameters used in the determination of detection limits for the different fragments produced from each compound are given in Table 3. The remainder of the

procedure was identical to that described for the LOD experiment using EI-FFS.

e. Precision and Linear Dynamic Range. The procedures used in the determination of linearity and precision did not differ from those previously described for EI-FFS (pp. 39-40). The experimental parameters used for each experiment are summarized by Table 3.

D. Two-Laser Experiments

1. Instrumentation

a. Probe Laser. In the LP-FFS experiments that involved the use of a second laser to "probe" the fragments produced by the photolysis laser, the probe laser was a Nd:YAG-pumped dye laser (Pump laser: DCR-2A10; dye laser: PDL-2; Quanta Ray, Mountain View, CA). The Quanta Ray laser system was equipped with a Wavelength Extender (WEX) which was used in these experiments to frequency-double the dye beam and to sum-frequency mix the dye beam with the fundamental beam (1064 nm) of the pump laser. An MCI Motor Control Interface (Quanta Ray) was used to automatically scan the grating motor of the pulsed dye laser.

Energy measurements of the laser beams were made using thermopile-type laser power meter heads (Scientech, Boulder, CO) and a power meter control unit (Model 362002, Scientech). A volume absorber-power meter head (Model 38-0101) was used to measure energies of the second harmonic (SH) of the Nd:YAG fundamental beam and dye laser beams. A surface absorber-power meter head (Model 36-0001) was used to measure energies of laser beams generated in the WEX.

In every case, the second harmonic of the Nd:YAG laser was used to pump the dye laser. The energy of the SH at 532 nm was normally ~300 mJ/pulse at 10 Hz, the maximum energy of the SH over the time period in which these experiments were performed. The pulse duration of the SH was 6-7 ns.

For each molecular fragment investigated the pulsed dye laser, containing an appropriate solution of laser dye, and WEX were realigned to yield appropriate ranges of tunable probe laser radiation.

Tunable probe laser radiation in the vicinity of 336 nm was used for the excitation of ground state NH radicals to the excited $A^3\pi$ state. This range of frequencies was obtained by using a mixture of the dyes DCM and LDS-698 in the dye laser. The dye concentrations in the oscillator and amplifier were 175 mg/L and 48 mg/L, respectively, for DCM and 40 mg/L and 10 mg/L, respectively, for LDS-698 in methanol. The dye beam was frequency doubled in the WEX. A wavelength range of approximately 620-680 nm from the dye laser could be frequency doubled to produce UV laser radiation over a range of approximately 310-340 nm. The dye laser was aligned with a 2.5-ns optical delay line and a preamplifier dye cell. The purpose of the optical delay line, positioned between the oscillator and preamplifier dye cells, was to minimize Amplified Spontaneous Emission (ASE) generated at the preamplier dye cell. The dye amplifier cell was longitudinally pumped. The λ^{max} for the dye beam was approximately 652.5 nm which corresponded to an energy of ~45 mJ/pulse; when frequency doubled to ~326 nm the measured energy was ~4.8 mJ/pulse. The energy of the UV beam at 336.0 nm was 3.6 mJ/pulse.

The dye Sulphorhodamine 640 was used for probing the CN radical. Oscillator and amplifier concentrations of 240 mg/L and 36 mg/L, respectively, were used in the dye laser with the solvent methanol. The resultant dye beam was mixed with the fundamental frequency from the Nd:YAG in the WEX to produce tunable UV radiation near 388 nm. The range in dye laser wavelengths that could be efficiently frequency-summed was approximately from 603 to 612 nm. The corresponding range of wavelengths from the WEX was approximately 385-388.5 nm. The dye laser was aligned using the 2.5-ns optical delay line and with longitudinal pumping of the dye amplifier cell. An energy of 65 mJ/pulse was obtained at a λ^{max} of 608 nm for Sulphorhodamine 640. The corresponding energy of the UV beam was ~6.3 mJ/pulse at 387 nm.

In order to generate tunable laser radiation appropriate for probing the CH fragment the dye LDS-750, in methanol, was used. The resultant dye beam was sum frequency-mixed with the Nd:YAG fundamental beam to produce a tuning range from 425-435 nm (λ^{max} = 431 nm). LDS-750 is a low-gain dye; thus the energy of the frequency-summed beam corresponding to λ^{max} for LDS-750 was only ca. 2 mJ/pulse. The dye concentrations were 115 mg/L and 15 mg/L for the oscillator and amplifier, respectively. The dye laser was aligned to include the 2.5-ns optical delay line, the preamplifier dye cell, and a longitudinally pumped amplifier dye cell.

b. Alignment of the Probe Laser Beam. The probe laser beam was aligned parallel and counter-propagating to the photolysis laser beam using two reflective mirrors (100% reflection at 337 nm) mounted on a

beam steering assembly (Model 111, Daedel, Harrison City, PA). Horizontal and vertical adjustments of the beam position could be made either at these mirrors or at the Pellin-Broca prism mounted just inside the exit port of the WEX. The probe beam passed through a stainless steel iris diaphragm with an aperture diameter approximately equal to the outer diameter of the beam, ca. 0.7 cm. The iris diaphragm was positioned approximately 5 cm in front of the fused silica window of the vacuum chamber.

The probe beam was positioned inside the laser photolysis-vacuum chamber such that it passed just beneath the terminus of the sample introduction tube. Aids for beam alignment were the image of the probe beam as seen at a white business card placed on the other side of the chamber and the back-reflections of the beam from the surfaces of the fused silica windows. An outline of the sample introduction tube could be seen at the image of the beam at the card. The beam was positioned beneath the tube such that the outline of approximately 1-3 mm of the tube was still visible. Back-reflections of the probe beam from the window of the chamber were used to obtain an alignment of the beam with little or no horizontal or vertical angle between the second beam-steering mirror and the window of the chamber.

Because the amount of laser light scattered by the tube could be unacceptably large it was necessary to block the top portion of the probe beam. This was accomplished by attaching a square plate of absorbing glass to the iris diaphragm using double-sided mounting tape. With the beam positioned with respect to the sample introduction tube

as described above, when the top of the beam was cropped, the most intense portion of the probe beam was positioned approximately 3 mm beneath the terminus of the tube as shown in Figure 7. Approximately one-quarter to one-third of the probe beam was blocked before entering the vacuum chamber.

c. Two-Laser Synchronization. In the two-laser experiments, the excimer laser is referred to as the "photolysis laser" and the Nd:YAG laser is referred to as the "probe laser." The photolysis and probe lasers were synchronized by the use of a variable delay circuit that was controlled by a multi-turn potentiometer. Briefly, this circuit was triggered by the down-going edge of the Nd:YAG flashlamp output pulse. The variable delay circuit could produce a signal pulse anywhere from 3.52-4.64 μs after the circuit was triggered. The up-going edge of this pulse triggered the photolysis laser which then fired after a 1.06 μs delay. The net result was that the photolysis laser could be fired either before or after the probe laser by a nominal value of 1000 ns. The timing jitter in pulses from the photolysis laser when triggered in this manner was estimated to be 15-20 ns. The photolysis laser, when used with the probe laser in this scheme, had to be operated with its trigger and COMMAND CHARGE selection switches at positions corresponding to EXTERNAL and OFF, respectively, or else its timing characteristics would be changed.

d. Measurement of the Two-Laser Time Delay. Two UV-photodiodes were used in conjunction with an oscilloscope (Tektronix Model 7854,

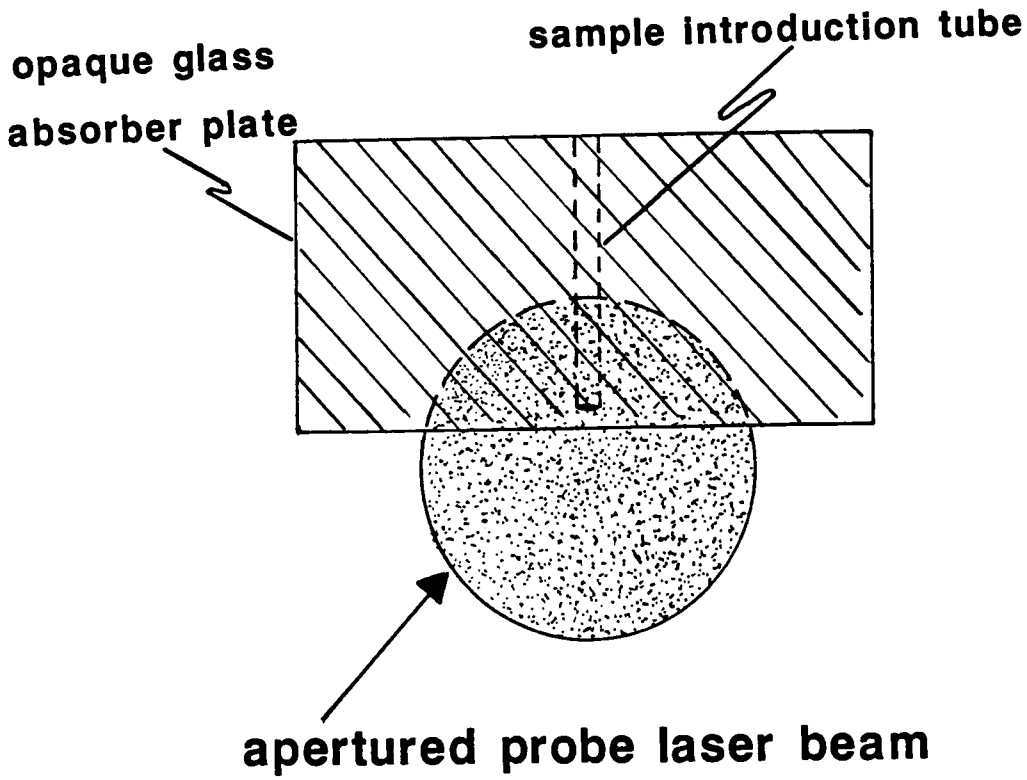

Figure 7. Diagram of shape of probe laser beam at sample introduction tube. Aperturing and cropping of beam are external to the photolysis chamber.

vertical unit: 7A26; horizontal unit: 7B53A) to measure the temporal difference between the photolysis and probe laser pulses as determined by the setting of the variable delay circuit. A photodiode was placed at the edge of each laser beam path and electrical connections were made between each photodiode and a channel of the dual-channel oscilloscope. An accurate measurement of the difference in the temporal firing of the two lasers (the two-laser delay time) could only be obtained if the response and recovery times of the photodiodes were sufficiently fast to track the narrow pulsewidths (<20 ns) of the lasers. In order to achieve this condition, the UV-040BQ photodiodes were biased with a voltage of 9V. A 9V-battery was connected to each photodiode in series with a 40-ohm load resistor. A circuit diagram of the biased photodiode is shown in Figure 8. The risetimes of the leading edges of both lasers were measured to be approximately 5 ns with ≤5 ns timing jitter using a time-scale of 100 ns/division.

2. Experimental Procedures

a. Introduction. The experimental parameters and procedures used in the two-laser experiments were much the same as for the laser photolysis, or one-laser, experiments. In initial attempts to increase fluorescence intensities by the use of the probe laser, two additional experimental parameters had to be considered: the excitation wavelength and the synchronization of the two lasers and the boxcar averager.

In these experiments, it was of interest to be able to perform resonance laser induced fluorescence, that is, an LIF experiment

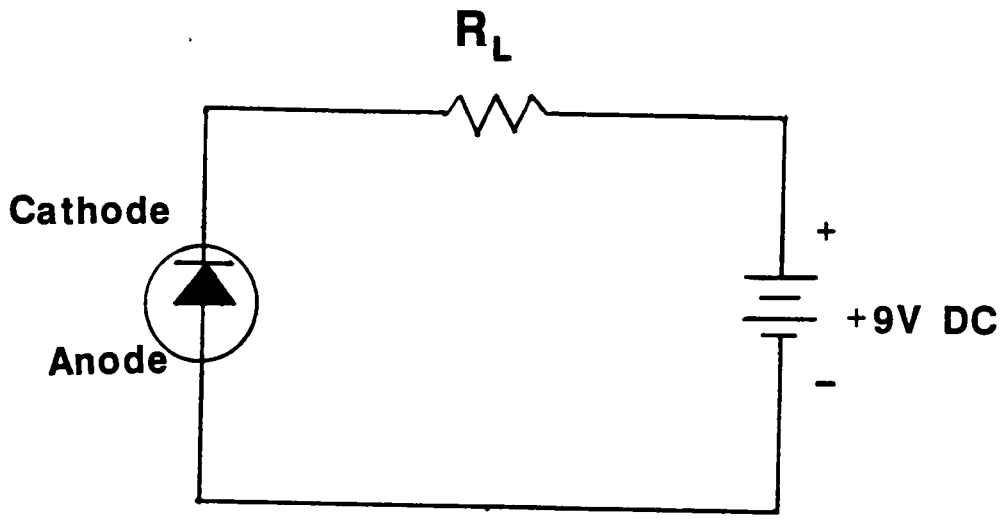

Figure 8. Circuit diagram of UV-photodiode with bias voltage applied to the cathode.

whereby the excitation wavelength and the emission wavelength are the same. At pressures typically used in these experiments, the rate of molecular collisions was low; thus the usefulness of exciting at one wavelength and detecting emission at another wavelength, an advantage of conventional fluorescence techniques, was presumed to be limited.

Under conditions of resonant excitation the scattered probe laser light imposed certain experimental restrictions. The intensity of the scattered probe laser light could not be so large as to make it difficult or impossible to measure a small LIF signal at the same wavelength. For fragments having fluorescence lifetimes in excess of approximately 50 ns, the boxcar averager could be used to resolve the fluorescence from the scattered light if a judicious selection of boxcar delay time was made. The synchronization of the two laser pulses was such that the probe laser pulse always followed the photolysis laser pulse but within a minimal time interval since the goal of these studies was to excite additional fluorescence from ground-state fragments that were initially formed, not from those that were the result of radiative decay from the excited state. Again, the synchronization of the boxcar gate vis-a-vis the firing of the lasers was critical in that the boxcar delay time had to be adjusted to enable the detection of fluorescence induced by the probe laser. A timing diagram of the two lasers and the boxcar averager is shown in Figure 9. The delay times of Figure 9 were typical values for the detection of CN fluorescence.

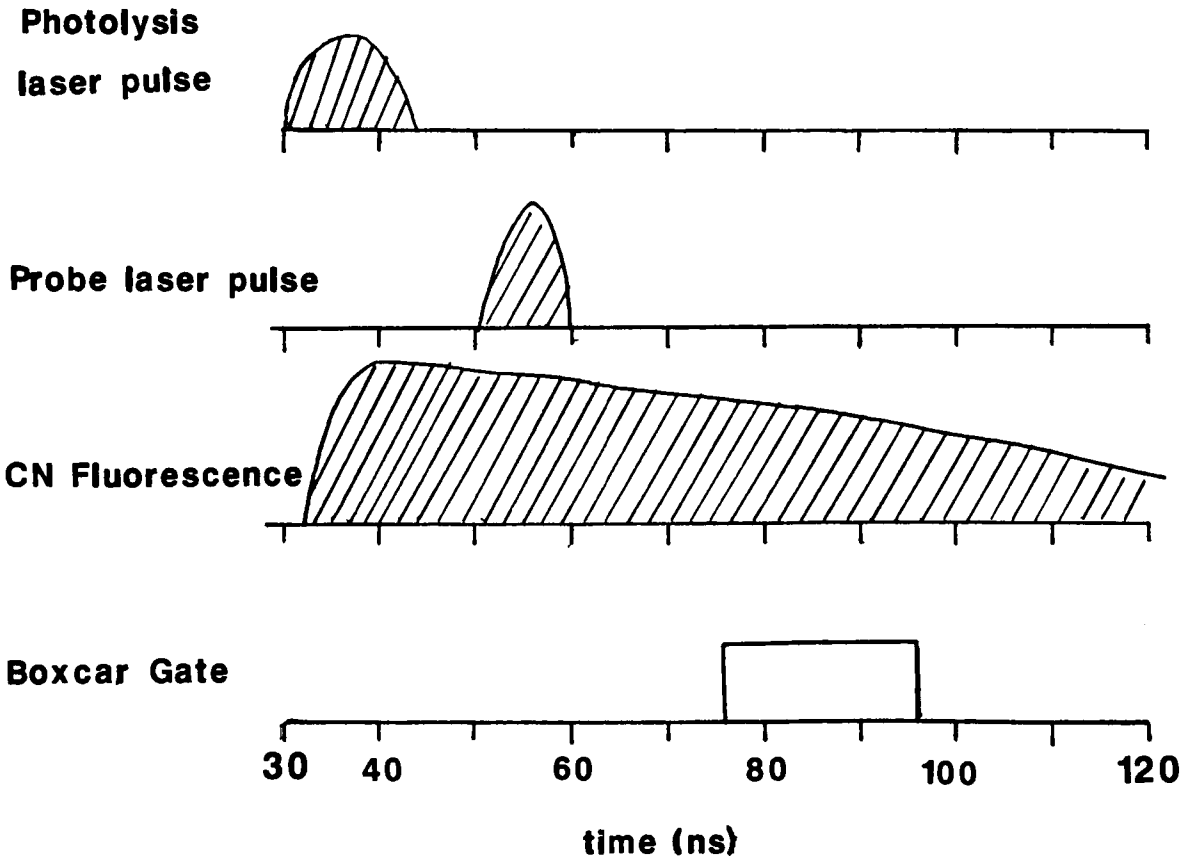

Figure 9. Timing diagram showing synchronization of photolysis and probe lasers and boxcar gate. The labeling of the time scale takes into account a propogation delay time of ca. 30 ns.

b. Two-Laser Synchronization. As an independent means of confirming the accuracy of the measurement of the 2-laser delay time using the 400 MHz oscilloscope and the modified UV-photodiodes, an experiment was devised whereby the same measurement was made using the boxcar gate scanner and is described below.

Of the two laser pulses, only the firing of the photolysis laser could be varied in time. Also, the photomultiplier tube was insensitive to the presence of scattered light from the photolysis laser at 193 nm. On the other hand, the scattered light from the probe laser, being of the visible or near-ultraviolet regions, was readily detectable using the PMT and boxcar averager. The signal due to the scattered light of the probe laser thus provided a temporal reference point from which the two-laser delay time could be measured. The boxcar averager and gate scanner were connected. In this configuration the boxcar-averaged output could be observed as a function of increasing boxcar delay time and the result was referred to as a "gate scan." The photolysis laser was used to trigger the boxcar during subsequent gate scans of the probe laser signal. Any change in the setting of the variable delay circuit was reflected by the time that the probe laser signal occurred in the boxcar gate scan. For each setting of the variable delay circuit the two-laser delay time was measured using the oscilloscope and the gate scanner. The two values of two-laser delay time were found to agree to within 20 ns for 8 different settings of the variable delay circuit (Appendix, Table A-1). The measurements obtained from the gate scan always exceeded those obtained using the oscilloscope by 5-20 ns.

In the experiments that follow, it was both more convenient and informative to use the boxcar gate scanner to synchronize the timing of the two lasers.

Three different types of boxcar gate scans were performed prior to each excitation or emission experiment to establish the two-laser delay time. An appropriate boxcar delay time was established at that time as well. These procedures were carried out for each experiment or set of experiments because the temporal relationship between the two lasers could not be maintained from day to day. Either the interruption of power or a trigger signal to the variable delay circuit could result in a significant change in the two-laser delay time. Boxcar gate scans for a typical set of gate scanning experiments are shown in Figure 10.

With the boxcar being triggered by the photolysis laser, a gate scan of the fragment fluorescence of interest was recorded. From this gate scan the boxcar delay time corresponding to maximum fluorescence intensity, t^{max}_F, could be obtained. A boxcar gate width of only 5 ns was used in order to enhance the resolution of any features of the scan. The monochromator was then tuned to transmit the probe laser wavelength and a second gate scan of the scattered laser light was performed. The variable delay circuit was adjusted to position the signal from the scattered light to follow t^{max}_F by approximately 10-20 ns. Since it was desirable for the probe laser pulse to be preceded by the photolysis laser pulse, the probe laser pulse was positioned in time relative to the fluorescence induced by the photolysis laser pulse. However, the probe laser pulse was delayed

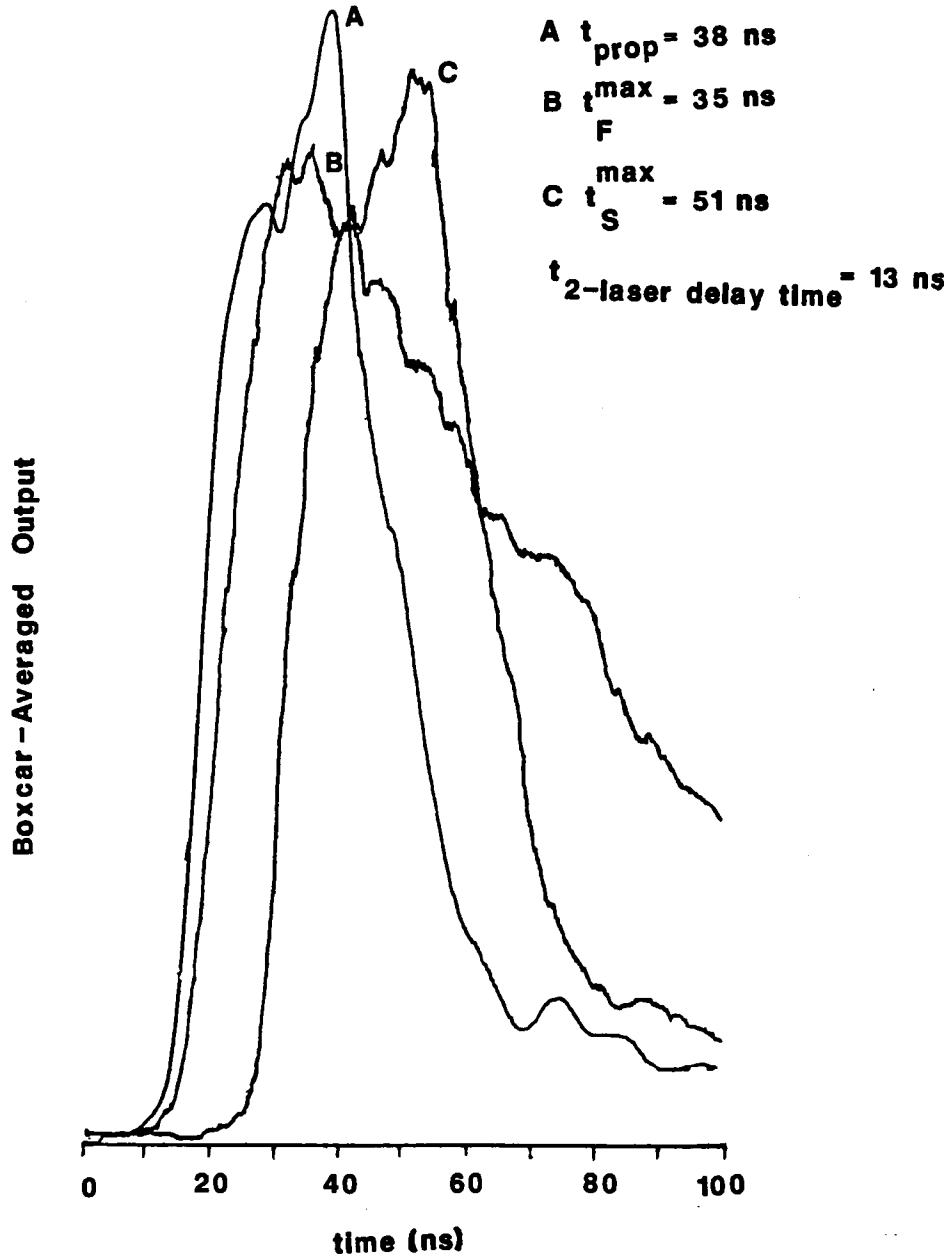

Figure 10. Boxcar gate scans used to establish two-laser synchronization for LIF excitation of CN fragment; t_{prop} = propagation delay time; t^{max}_{F} = time corresponding to maximum CN fluorescence induced by the photolysis laser; t^{max}_{S} = time corresponding to maximum intensity of probe laser scattered light; $t_{2\text{-laser delay}} = t^{max}_{S} - t_{prop}$; λ^{mon}_{CN} = 388.3 nm; $\lambda^{mon}_{probe\ laser}$ = 386.5 nm.

relative to the incidence of the maximum fluorescence intensity so as to take into account the timing jitter of the photolysis laser. The subsequent gate scan yielded the time corresponding to the maximum intensity of scattered probe laser radiation or t^{max}_s. When the photolysis laser was used to trigger the boxcar averager, t^{max}_s consisted of the two-laser delay time plus the time it takes for the scattered light signal to reach the boxcar, the so-called propagation delay time, or t_{prop}. To estimate the magnitude of t_{prop}, a second gate scan of the scattered probe laser radiation was performed; this time the probe laser itself was used to trigger the boxcar averager. As scattered laser light occurs instantaneously, a signal obtained in this manner was taken to approximate the combined electronic propagation time of the signal through the PMT and boxcar averager. The two-laser delay time could then be estimated by subtracting the value of t_{prop} from that of t^{max}_s.

The probe laser beam was left as the trigger signal to the boxcar. This was done for several reasons. There is less timing jitter associated with the probe laser pulse than with the photolysis laser pulse due to the greater pulse-to-pulse amplitude instability of the latter. This produces a less noisy boxcar-averaged output. Also, the probe laser pulse, being stationary in time, resulted in a boxcar-averaged output that was always constant, in time, relative to the probe laser scattered light whose contribution to background could be quite large and varied as a function of time. This method of triggering the boxcar should also have made it easier to detect any fluorescence induced by the probe laser.

The final part of the procedure to establish the two-laser synchronization was to position the boxcar gate relative to the incidence of the scattered probe laser signal. Without making any other changes to the apparatus, the gate scanner was disconnected from the boxcar averager and the boxcar delay time was scanned by hand until the scattered light signal reached maximum intensity. The boxcar delay time was either left at this value or increased. The ultimate choice of a boxcar delay time was influenced by the fluorescence lifetime of the fragment under study and the possible need to invoke time-based discrimination against the background signal. After the boxcar delay time had been established, the width of the boxcar gate was adjusted to the previously determined value established for each fragment in the one-laser experiments and an excitation experiment was begun. Values for delay times used in the two-laser experiments are given in Table 4.

c. Laser-Induced Fluorescence Excitation Spectra. The purpose of performing LIF excitation experiments was to ascertain appropriate excitation wavelengths to be used in subsequent LIF emission spectra.

A trial scan of the probe laser wavelength was carried out for each range of excitation wavelengths prior to the LIF excition experiments. After proper alignment of the PDL-2 and WEX had been achieved, the MCI was used to scan the probe laser wavelength while the energy of the beam was measured using the power meter. The energy vs. wavelength measurements were made before the laser beam was cropped at the iris diaphragm. The laser energies measured for each wavelength scan are given in Table 5.

Table 4. Spectral and temporal parameters for LIF excitation experiments.

Fragment	Compound	λ_{em}[a] (nm)	λ_{exc} range (nm)	t_{delay} two-laser	t_{delay}[b] boxcar	Ref.
CN	$C_4H_9NH_2$	388.3	388.5-385.5	20 ns	0 ns	53,56
Cu	$Cu(hfa)_2 \cdot 2H_2O$	324.75	324.75	25 ns	2 ns	67,71
CN	$C_4H_9NH_2$	388.3	388.5-385.5	13 ns	24 ns	53,56
NH	CH_3NH_2	336.1	336.2-333.0	35 ns	30 ns	47
		337.1	337.2-335.0	35 ns	30 ns	45
		336.1	337.2-335.0	35 ns	30 ns	47
NH	$C_{14}H_{29}NH_2$	336.1	337.2-332.5	35 ns	30 ns	47
CH	$C_4H_9NH_2$	431.4	433.0-428.0	20 ns	20 ns	72

[a]Optimized for one-laser fluorescence.

[b]Relative boxcar delay time (boxcar delay time - t_{prop}^{hand}).

Table 5. Measurements of energy vs. wavelength for probe laser beam.

Fragment	λ^{ex} (nm)	Laser Energy (mJ/pulse)
CN	388.5	~3
	388.0	3.7
	387.5	5.0
	387.0	6.0
	386.5	6.6
	386.0	6.6
	385.5	5.6
	385.0	~3
Cu	324.75	5.2
NH	336.0	~3
	335.5	3.1
	335.0	3.3
	334.5	3.4
	334.0	3.4
	333.5	3.5
	333.0	3.6
CH	433	~0.3
	432	~0.3
	431	~0.3
	430	~0.3
	429	~0.3
	428	~0.3
	427	~0.3

The two-laser delay time and boxcar delay time were established as described in section II.D.2.a., above, just before the initial experiment of the day was begun. An excitation experiment consisted of scanning the excitation or probe laser wavelength while monitoring the fragment fluorescence at a particular wavelength using the emission monochromator. Monochromator slit widths of 100 μm were typical. The scan rate (~0.001 nm/s) of the excitation wavelength was slow enough to permit the boxcar to average signals over 100 laser shots per 0.01 nm scanned. The choices of the emission wavelength and the range of the excitation wavelength for each experiment was appropriate for the particular fragment being investigated. This information is summarized in Table 4. Blank excitation spectra, in which the experimental conditions were unchanged from those of the previous spectrum, were acquired in the absence of sample.

d. Laser-Induced Fluorescence Emission Spectra. The excitation experiments were followed by LIF emission experiments whereby the effect of the probe laser on the photolysis laser-induced emission spectrum could be assessed. While at a constant probe laser wavelength, the emission monochromator was scanned over an appropriate region of the fragment fluorescence spectrum. The emission spectrum may or may not have included the probe laser wavelength. The ranges of wavelengths of each fluorescence spectrum along with the excitation wavelength used in each experiment are summarized in Table 6.

In order to distinguish any background signal due to scattered probe laser light from fragment emission, the emission scans were

Table 6. Spectral parameters for LIF emission experiments.

Fragment	λ_{ex} (nm)	ν', ν'' Transition	λ_{em} range (nm)
CN	388.3	0,0	385.0-389.0
	387.14	1,1	
	386.20	2,2	
NH	336.1	0,0	334.0-338.0
	337.1	1,1	

acquired once with both lasers on and running and again without the photolysis laser. The difference in signal levels between the photolysis laser-induced fluorescence and the photolysis plus probe laser (two-laser) fluorescence was discerned by repeating the emission scan a second time with the probe beam blocked before it entered the photolysis chamber. Sample was present at a constant pressure throughout the acquisition of each emission spectrum.

Emission spectra of a LIF signal from atomic copper were used to optimize the position of the probe beam with respect to the sample introduction tube. This was accomplished by acquiring an emission spectrum, with and without the photolysis laser running, for each change that was made in the position of the beam. Each pair of spectra enabled relative changes in the LIF signal to be assessed, as the intensity of the scattered laser light at the same wavelength was also dependent upon the position of the probe laser.

CHAPTER III

RESULTS AND DISCUSSION

A. Introduction

A summary of the quantitative results of analyses of all compounds by EI- and LP-FFS are given in Tables 7 and 8, respectively. The discussion of the results that follows is organized according to the compound analyzed.

B. Ammonia

1. Electron Impact

Figure 11 shows the fragment emission spectrum produced by electron impact of ammonia. The spectrum contains emissions from the fragments NH and H. Two fluorescent systems are observed for the NH fragment, the $A^3\pi$-$X^3\Sigma$ at ca. 336 nm and the $c^1\pi$ -$a^1\Delta$ occurring in the region from 324.0-340.0 nm. Four transitions in the H-Balmer series are detected at relatively high S/N, $H\epsilon$, $H\delta$, $H\gamma$, and H_β, corresponding to the wavelengths 397, 410, 435, and 486.5 nm, respectively. These assignments were made based on the work of Johnson (21). The results are very similar to those observed by previous workers (15,17,18,20,22,23).

The emission bands seen near 391 and 428 nm are due to $N_2^+(B^2\Sigma^+$-$X^2\Sigma^+)$ 0,0 and 0,1 transitions, respectively, while the emission at 358 nm is attributed to the $N_2(C^3\pi$-$B^3\pi)$ 0,1 transition (28). These emission

Table 7. Quantitative results for EI-FFS.

Compound	Fragment (transition), λ	LOD[a]	LOD	LDR	RSD
N_2	N_2^+ ($B^2\Sigma$-$X^2\Sigma$), 391nm	$5x10^{-8}$	10 pmol	3 decades	1.0%
NH_3	NH ($A^3\pi$-$X^3\Sigma$), 336nm	$1x10^{-7}$	20 pmol	3 decades	1.4%
CH_3NH_2	H_β (n=4-n=2), 486nm	$1.5x10^{-6}$	300 pmol	2 decades	1.2%
CH_3CN	CN ($B^2\Sigma$-$X^2\Sigma$), 388nm	$6x10^{-7}$	100 pmol	2 decades	1.2%

[a]In torr (1 torr = 3.23 x 10^{16} molecules/cm^3).

Table 8. Quantitative results for LP-FFS at 193 nm, based on CN ($B^2\Sigma \rightarrow X^2\Sigma$) fluorescence at 388.3 nm.

Compound	MW	LOD, torr	LOD	LOD	LDR	RSD, %
NH_3	17	$9x10^{-8}$	0.037 ng	2.2 pmol	1 decade $1x10^{-7}$ - $2x10^{-6}$	6.1
CH_3NH_2	31	$3x10^{-7}$	0.5 ng	15 pmol	3 decades $3x10^{-7}$ - $3x10^{-4}$	6.1
$n\text{-}C_4H_9NH_2$	73	$1x10^{-6}$	2 ng	26 pmol	2.5 decades $1x10^{-6}$ - $5x10^{-4}$	4.9
$(C_2H_5)_2NH$	73	$2x10^{-6}$	3 ng	44 pmol	2.5 decades $1x10^{-6}$ - $5x10^{-4}$	6.8
$n\text{-}C_6H_{13}NH_2$	101	$2x10^{-6}$	4 ng	40 pmol	2.5 decades $2x10^{-6}$ - $6x10^{-4}$	7.3
$(C_4H_9)_2NH$	129	$8x10^{-7}$	3 ng	20 pmol	2.5 decades $1x10^{-6}$ - $4x10^{-4}$	5.1
$(C_4H_9)_3N$	185	$3x10^{-6}$	12 ng	70 pmol	1.7 decades $2x10^{-6}$ - $1x10^{-4}$	4.5
$n\text{-}C_{14}H_{29}NH_2$	213	$4x10^{-6}$	20 ng	100 pmol	1.5 decades $2x10^{-6}$ - $5x10^{-5}$	ND
$n\text{-}C_{16}H_{33}NH_2$	241	$2x10^{-6}$	10 ng	41 pmol	ND	ND

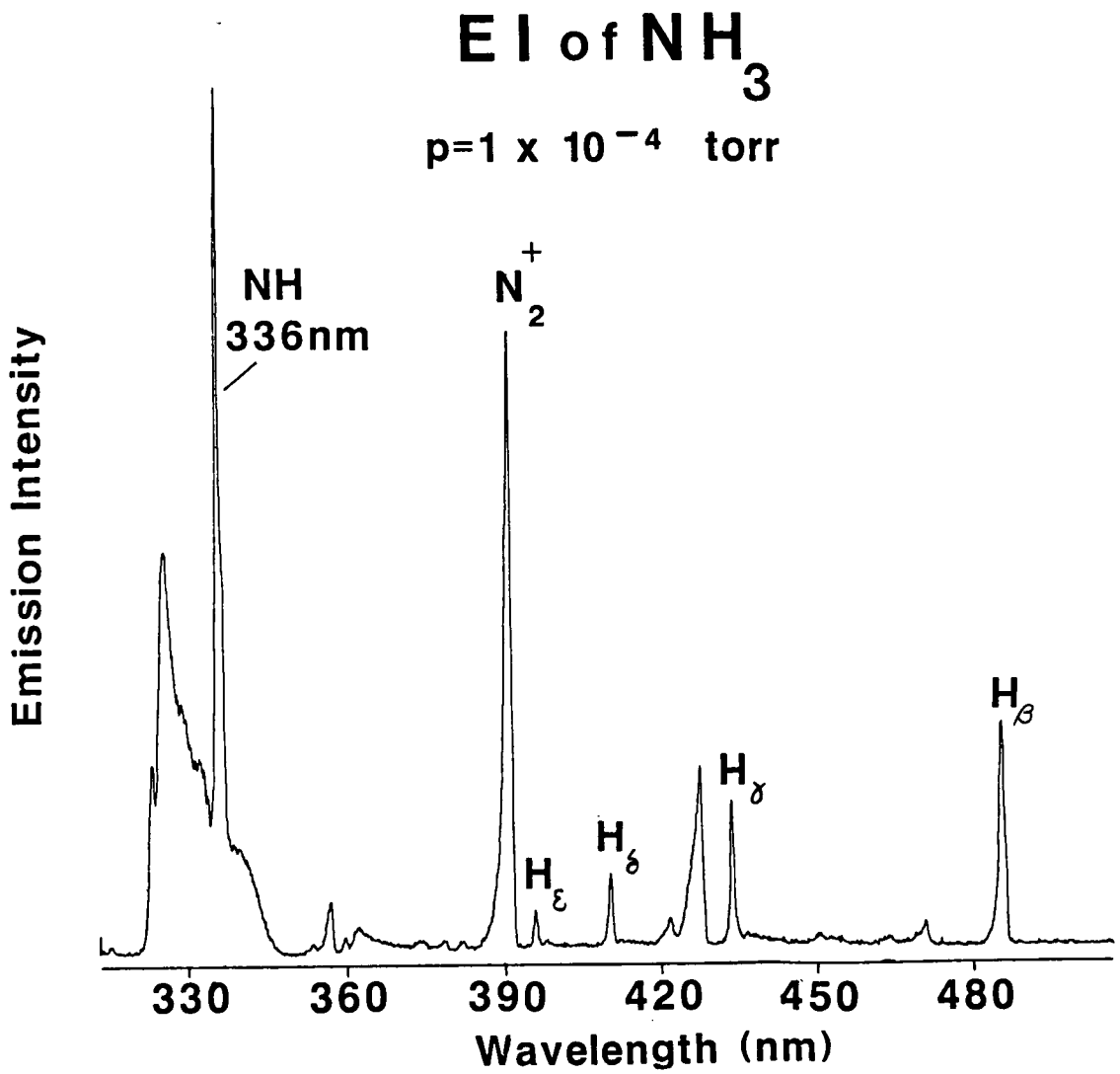

Figure 11. EI-FFS emission spectrum of ammonia.

bands indicate that the gaseous sample of NH_3 was contaminated with N_2, as neither a blank emission scan nor the base pressure of the vacuum system (6×10^{-8} torr) indicated the presence of a leak from atmosphere.

The most intense emissive feature produced by the electron-impact fragmentation of ammonia is that due to NH(A-X) 0,0 and 1,1 vibronic transitions. The emission intensity of this system as shown in the survey spectrum of Figure 11 is ~7,500 cps. The 0,0 transition at 336.0 nm and 1,1 transition at 337.0 nm are not resolved under these experimental conditions; however, the position of the peak maximum indicates that the 0,0 transition produces the more intense emission. These results are consistent with those found by other investigators (15,17,18,20-25).

The limit of detection for ammonia was determined to be 1×10^{-7} torr or 3.2×10^{9} molecules/cm^3 (S/N = 3) using the NH(A-X) 0,0 transition near 336 nm. This is the value obtained after correcting for the differences in the response between the two pressure measurement devices. The corresponding uncorrected or ionization gauge (IG) pressure was 3×10^{-7} torr. The absolute detection limit was calculated to be 0.36 ng or 21 pmoles.

The emission signal near 336 nm was found to be linear over the entire pressure range studied, from 4×10^{-7} to 8×10^{-4} torr, with a correlation coefficient of 0.9936. The relative standard deviation of the slope of the analytical calibration curve was determined to be 3.0%.

The analytical precision expressed as percent relative standard deviation was determined to be 1.4% for 11 replicate measurements at a sample pressure of 1×10^{-6} torr.

2. Laser Photolysis

Figure 12 is a survey spectral scan of the laser-photolysis fragment fluorescence produced by ammonia in the region from 315 to 515 nm. Fluorescence due only to one NH system was observed as opposed to the much more complex electron-impact survey spectrum of ammonia. The emission band ranging from ca. 330-343 nm is due to NH($A^3\pi$-$X^3\Sigma$) and has been reported by previous workers (38,41,42,45,46). The Q(0,0) transition belonging to this system appears as the narrow, intense peak seen at 336 nm. The much more weakly intense Q(1,1) transition is cleanly resolved from the Q(0,0) transition and is measured at 337 nm. The emission band due to NH($b^1\Sigma$-$x^3\Sigma$) at 470.8 nm reported by MacDonald (38) was not seen under the conditions of this experiment.

The noise which occurs in the remainder of the LP survey spectrum for ammonia in the region from ca. 334 to 444 nm was determined by a blank spectral scan to be background fluorescence. The most probable source of this signal was a residue which remained in the photolysis chamber after the LP-FFS analysis of a copper chelate by another user of the instrument.

The dependence of the NH(A) fluorescence signal on laser power for ammonia indicates that the rate-determining steps of photon absorption involved in the production of NH(A) were somewhat saturated even at relatively low laser energies. This conclusion is based on the determination by previous workers (38,43,44) that two 193-nm photons are required in the production of NH(A) from ammonia. Accordingly, the

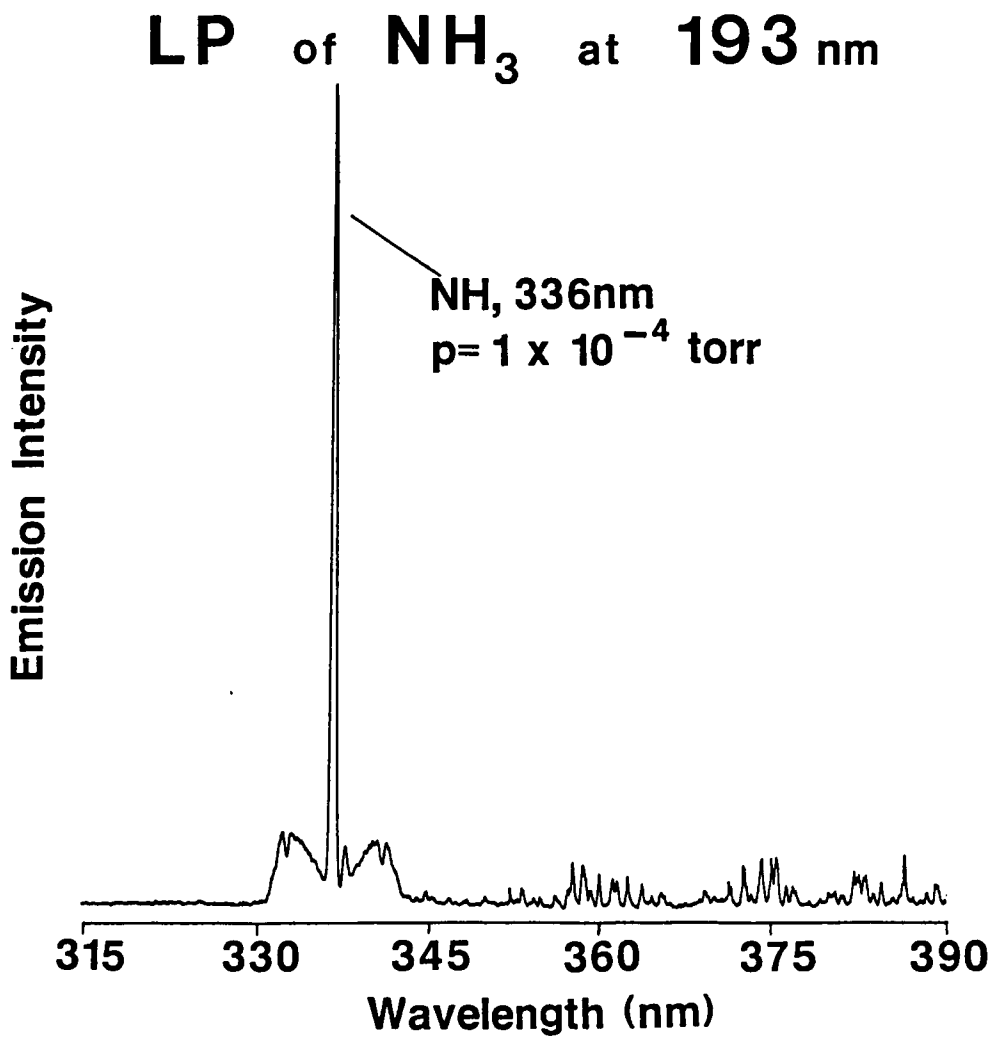

Figure 12. LP-FFS emission spectrum of ammonia.

theoretical dependence of this fragment fluorescence signal on laser energy would be quadratic. These experiments yielded a signal dependence on laser pulse energy of 1.4 power for laser energies of 30 to 40 mJ/pulse. As the laser energy was increased a much higher degree of saturation was indicated. A power index of approximately 0.2 was obtained at laser energies from 40 to 120 mJ/pulse. The study was repeated, with replicate scans acquired for each laser energy setting, and the average values for each group of scans were used to construct the power-dependence plot. For laser energies of 30 to 40 mJ/pulse the plot yielded a power index of approximately 1.2, from 40 to 60 mJ/pulse, 0; and for 60 to 115 mJ/pulse, approximately -0.5. Based on the results of both studies, a laser energy of 50 mJ/pulse was chosen as the optimum photolysis energy for subsequent quantitative experiments.

The detection limit for ammonia based on NH(A-X)0,0 fluorescence was estimated to be approximately 9×10^{-8} torr or 3×10^{9} molecules/cm^3 (S/N = 2) after correcting for the response of the pressure gauge. Based on the volume of the vacuum chamber the absolute detection limit was calculated to be 37 pg or 2.2 pmoles. The sensitivity for detection of NH_3 by laser photolysis is about one order of magnitude higher than that achieved by electron impact.

The emission due to NH(A-X) was linear in ammonia pressure over a limited range, from ~1×10^{-7} to 2.5×10^{-6} torr. A rather severe negative deviation from linearity was seen at pressures greater than

the upper limit of this range. A second linear dynamic range study, including 4 replicate scans at each pressure, confirmed these findings.

These results are probably due to quenching of NH(A) by chemical recombination reactions since the rate of 2-body collisions increases with pressure. An alternate explanation of the results is that they could be caused by self-absorption of the emitted radiation by ground-state NH fragments. The lack of any similar trends in the corresponding data for electron impact partially supports the former argument. If one assumes that ground state NH is produced by both EI and LP, then evidence of self-absorption might occur for both techniques. However, owing to the inherent differences in the two fragmentation techniques, one should expect that they would produce different types and relative abundances of reactive fragments. Thus, it is conceivable that pressure-dependent reactions might not occur to the same extent in both instances.

The precision with which the NH(A)0,0 transition could be measured was 6.1% RSD for 16 replicate measurements at a sample pressure of ca. 3×10^{-5} torr. These measurements were made under conditions in which the power dependence of the NH(A-X) fluorescence was 0 (see Table 3, page 52).

C. Methylamine

1. Electron Impact

The electron-impact fragmentation fluorescence spectrum of methylamine is shown in Figure 13. Several different excited fragments were produced: $NH(A^3X)$, $CN(B^2\Sigma)$, $CH(A^2\Delta)$, and the H (Balmer series).

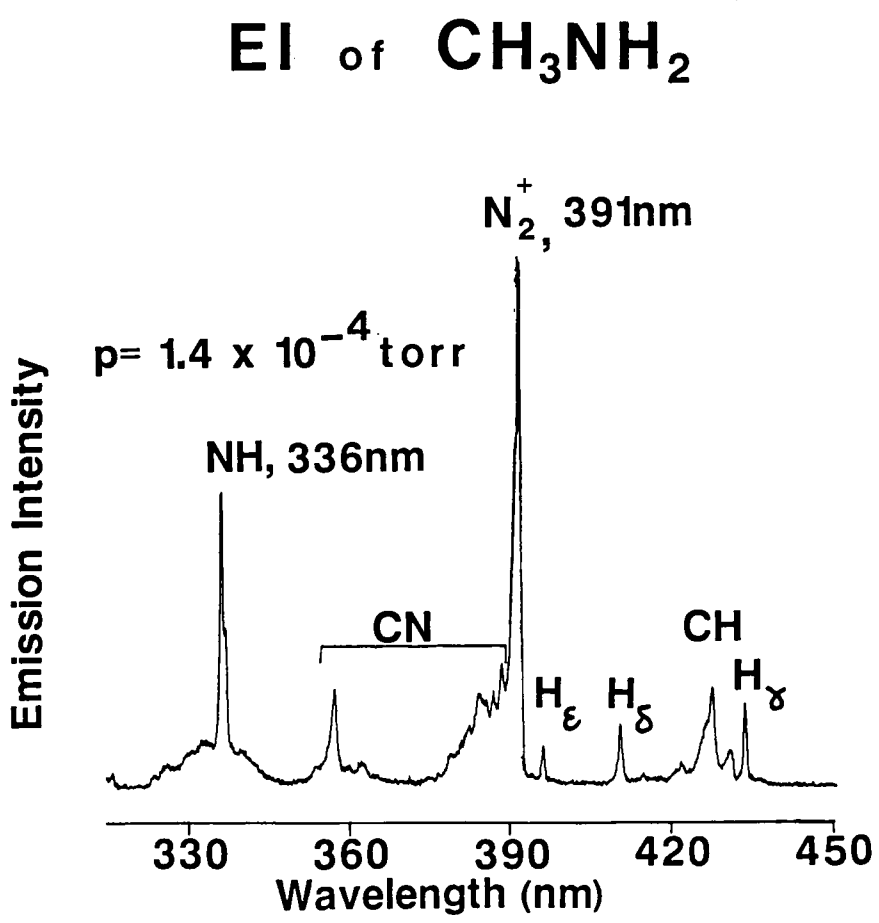

Figure 13. EI-FFS emission spectrum of methylamine.

There was very little, if any, detectable contribution to NH emission from the NH($c^1\pi$-$a^1\Delta$) system in the vicinity of 324 nm. The same excited species were observed by Fujita (19,18) and Johnson (21).

As was the case for ammonia, contamination of the gaseous methylamine by N_2 was significant. Fluorescence from the CN(B-X) system is subject to interferences from two N_2 emissions. The CN(B-X)1,0 and 0,0 bands at 359 and 388 nm, respectively, are very close to emission bands due to N_2(C-B)0,1 at 357.7 nm and N_2^+(B-X)0,0 and 1,1 transitions at 391.4 and at 388.4 nm, respectively. However, these interferences did not present a problem for the subsequent quantitative analysis of methylamine by EI-FFS because, of the fluorescent fragments produced, the emissions due to NH(A-X) and H_β are the most intense. The H_β-line at 486.5 nm (not shown in Figure 13), although not quite as intense as the NH(A-X) fluorescence under these experimental conditions, was used in the subsequent quantitative determinations of LOD, LDR, and precision because, unlike the NH emission, the H_β-line rises cleanly from the baseline. This condition simplified the task of reproducibly and accurately measuring the peak heights above background noise.

The detection limit of the H_β emission was found to correspond to a corrected pressure of 1.5×10^{-6} torr or 5×10^{10} molecules/cm^3 (S/N = 2) for methylamine. An absolute detection limit of 10 ng or 0.3 nmoles was calculated. The signal due to H_β emission was found to be linear in sample pressure over a range of more than two decades, from 8×10^{-7} to ca. 2×10^{-4} torr. Linear regression analysis of the data yielded a

correlation coefficient of 0.9977. The relative standard deviation of the slope of the calibration line was 2.6%.

The precision with which the H_β emission could be measured at a pressure of ~2 x 10^{-5} was estimated to be 1.2% RSD using 14 replicate emission scans by EI-FFS.

2. Laser Photolysis

The laser photofragmentation of methylamine resulted in the production of the excited fragments NH(A), CN(B), and CH(A) as is illustrated by the emission spectrum in Figure 14. The most intense emission produced from the laser-photofragmentation of methylamine was CN(B-X). This fluorescence system ranged from ~358 to 421 nm, with the maximum intensity due to the 0,0 transition occurring near 388 nm. The NH(A-X) fluorescence near 336 nm is observed at much lesser intensity than observed from either the laser photolysis of ammonia or the electron impact of methylamine. The least intense fragment emission is due to the excited species, CH(A). The emission due to the CH(A-X) system is centered around 431 nm and is degraded to the violet. The weakly intense peaks seen around 387 and 389 nm correspond to fluorescence produced by CH($A^2\Delta$-$X^2\pi$)0,0 transitions, although this assignment is ambiguous as there also exist transitions from the CN(B) violet system in this region (389, 390 and 392 nm) with relatively high intensities (11). Unlike the electron-impact spectrum for methylamine, no H-Balmer lines were produced by laser photofragmentation.

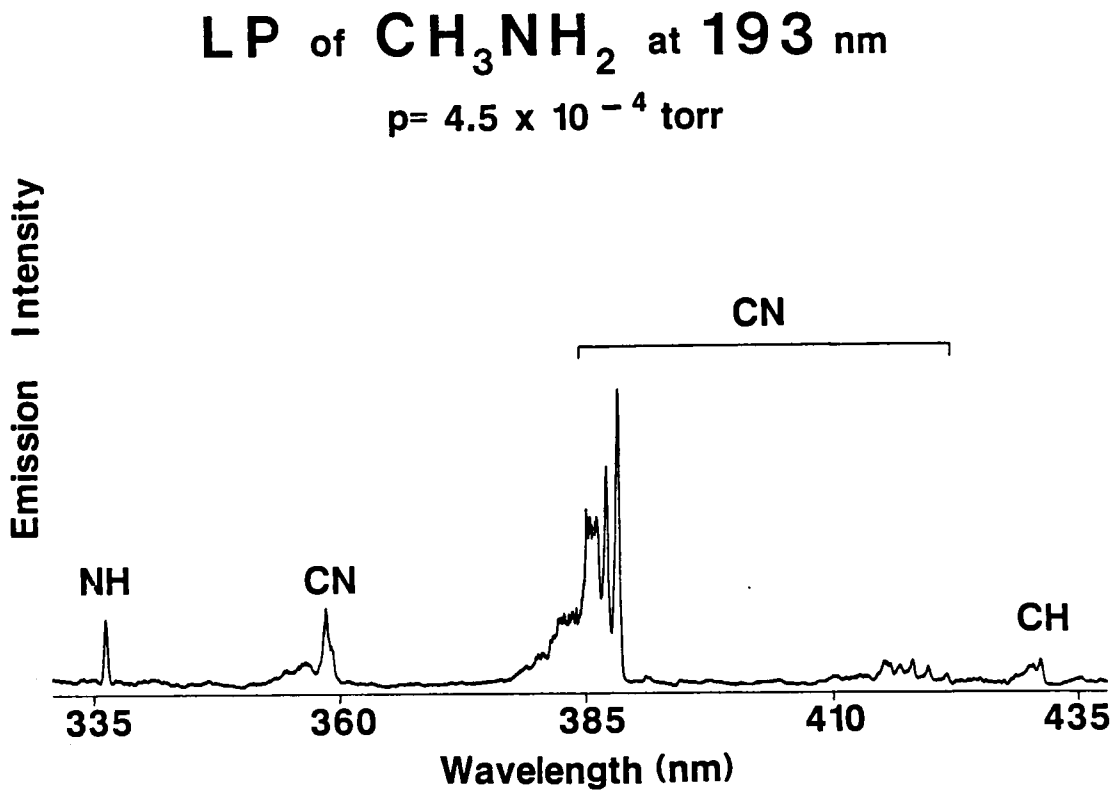

Figure 14. LP-FFS emission spectrum of methylamine.

The power dependence of CN(B-X)0,0 fluorescence intensity on pulse energy of the photolysis laser over the laser output range of 40 to 95 mJ/pulse was approximately 1. This result indicated that this transition was highly saturated as the theoretical power dependence based on the number of photons required for the production of CN(B) would be 3 (44,49). Based on the results of this study and the current functioning of the ArF excimer laser, an optimal laser energy of 55 mJ/pulse was selected for use in the remainder of the experiments involving the photofragmentation of methylamine.

The detection limit of methylamine based on the fluorescence due to CN(B-X)0,0 near 388 nm was estimated to be approximately 3×10^{-7} torr or 10×10^{9} molecules/cm^3 (S/N = 2), corresponding to an absolute detection limit of 0.5 ng or 15 pmoles. The uncorrected detection limit was 6×10^{-7} torr.

CN(B-X)0,0 fluorescence was found to be linear in methylamine pressure over approximately 3 orders of magnitude, from 1×10^{-7} to 2.7×10^{-4} torr. A slight negative deviation from linearity was exhibited at sample pressures in excess of 2.7×10^{-4} torr to the highest pressure studied, 5.3×10^{-4} torr. This is similar to what was seen for the laser photolytic linear dynamic range studies of ammonia and implies the probable occurrence of collisions at higher pressures. A correlation coefficient and relative standard deviation of 0.9897 and 4.0%, respectively, were calculated for the linear region of the slope of the calibration line.

The relative standard deviation of the fluorescence signal from the CN(B-X)0,0 transition was estimated to be 6.1% for 14 replicate measurements, the same estimate as was found for ammonia by LP-FFS. The methylamine pressure was 2 x 10^{-4} torr throughout this experiment.

D. n-Butylamine

1. Laser Photolysis

The laser-photolysis fragment fluorescence spectrum of n-butylamine contains emissions due to NH($A^3\pi$-$X^3\Sigma$), CN($B^2\Sigma$-$X^2\Sigma$), and CH(A^2 -$X^2\pi$), as shown in Figure 15. The CN(B-X) fluorescence is the most intense, followed by CH(A-X) fluorescence. Under the experimental conditions used (see Table 3, page 52) the fluorescence from the NH(A-X)0,0 transition appears as the very weak signal around 336 nm; otherwise the spectrum is very similar in appearance to the laser photolysis spectrum of methylamine.

For the power dependence study, a plot of log fluorescence intensity versus log laser power yielded a straight line with a slope of 1.8 over a range of laser energies from 50 to 100 mJ/pulse. Although there are no reports of the laser photolysis of any other primary alkylamines, one might expect a multiple-photon dependency which is consistent with that of methylamine, i.e., n = 3.

Given the nearly quadratic dependence of signal intensity on laser energy, the highest sensitivity would be achieved by operating at the maximum laser energy. However, a laser energy of 80 mJ/pulse was chosen for use in subsequent experiments as a value that would yield

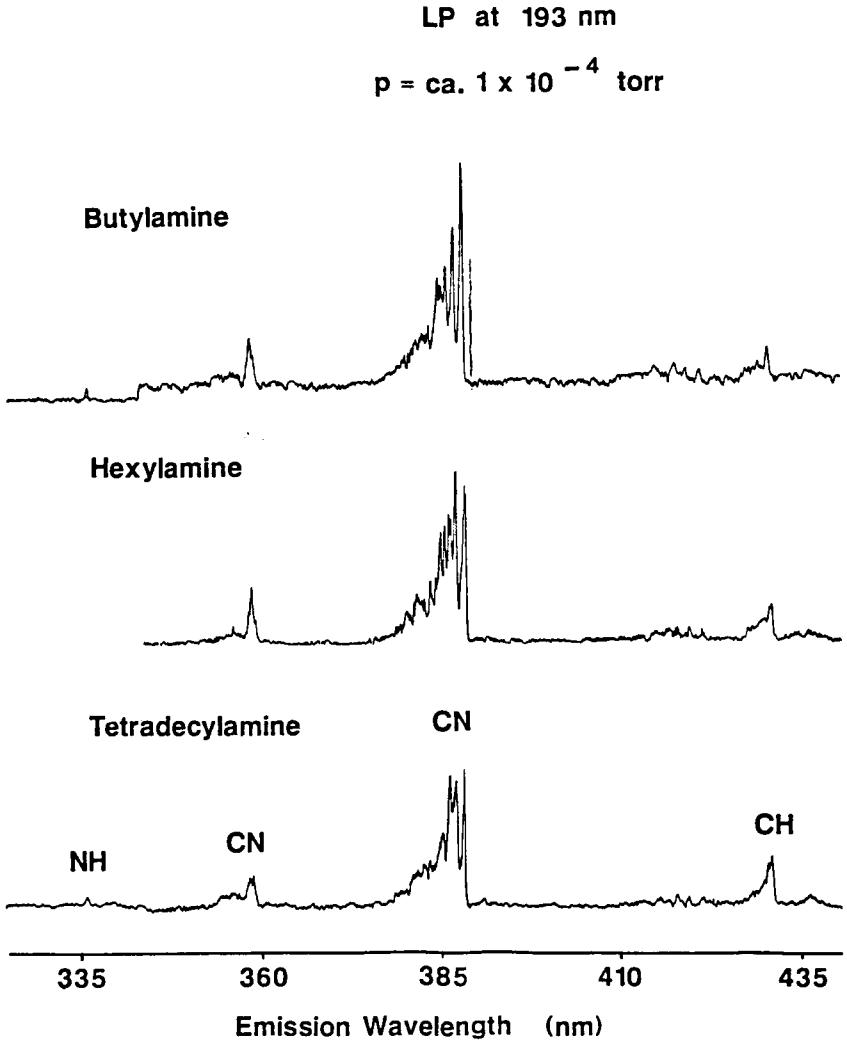

Figure 15. LP-FFS emission spectra of n-butylamine, n-hexylamine, and n-tetradecylamine.

relatively high S/N while allowing for some degradation of the laser performance with time.

The detection limit was determined to be 1.1×10^{-6} torr or 3.5×10^{10} molecules/cm^3 (S/N = 2.5, uncorrected). The detection limit expressed as absolute mass is 2 ng or 26 pmole, representing an increase over that determined for methylamine by a factor of ~2.

The range in butylamine pressure over which the CN(B) emission was found to be linear was from ca. 1×10^{-6} to 5×10^{-4} torr (2.5 decades). The results of the linear regression analysis of the analytical calibration line yielded a correlation coefficient of 0.9816 and 4.7% RSD for the slope.

The precision of measurement was estimated to be 4.8% RSD for 12 replicate measurements of the CN(B-X)0,0 fragment emission at a pressure of 1.2×10^{-5} torr.

E. n-Hexylamine

1. Laser Photolysis

The fragment fluorescence spectrum produced by the laser photolysis of hexylamine was very similar to that yielded by butylamine (Figure 15). The same fragments appear in the emission spectra of both compounds and with virtually the same relative intensities. The experimental conditions with which both spectra were acquired are very similar.

There was only a small increase in the detection limit for CN(B) emission at a S/N of ~2.5 in going from butyl- to hexylamine, from 1.1

x 10^{-6} to 1.7 x 10^{-6} torr, respectively. The detection limit expressed as molecules per cm^3 was 5.5 x 10^{10} and in terms of absolute mass was 40 pmole (an increase relative to methylamine of less than a factor of two).

The results of the linear dynamic range studies for the butylamine and hexylamine were very similar. The linear range of CN(B) emission intensity with hexylamine pressure was from 2 x 10^{-6} to ca. 6 x 10^{-4} torr. The calibration line over this range was determined by linear regression analysis to have a correlation coefficient of 0.9988. The relative standard deviation of the slope of the calibration plot was 1.4%.

The precision of measurement was estimated to be 7.3% using 11 replicate emission scans of the CN(B-X)0,0 fluorescence signal at a hexylamine pressure of 3.2 x 10^{-5} torr.

F. n-Tetradecylamine

1. Laser Photolysis

The emission spectrum produced by the laser photolysis of tetradecylamine is shown in Figure 15. The same excited fragments were observed as for methyl-, butyl-, and hexylamine; however, the relative intensity of the emission from CH(A) was increased and that from CN(B) was decreased.

The detection limit obtained for tetradecylamine using the most intense CN fragment emission was 4 x 10^{-6} torr or 1.3 x 10^{11} molecules/cm^3 (uncorrected, S/N = 2). The corresponding absolute

detection limit was 100 pmole, representing the highest LOD obtained to date by LP-FFS. The range in sample pressure over which this signal was found to be linear was from 1.7×10^{-6} to ca. 5×10^{-5} torr (~1.5 decades). The linear range was limited on the low pressure extreme by the ability to detect the emission band with a S/N of at least 1.5 and on the high pressure extreme by the vapor pressure of the sample. The latter was limited by the temperature to which the sample introduction system could safely be heated. The correlation coefficient obtained by linear regression analysis was 0.9769. The relative standard deviation for the slope of the plot was found to be 10.9%; however, this analysis was based on only 6 data pairs within the linear region of the curve. The relatively large variance of the calibration line can also be attributed to the difficulty encountered in obtaining stable sample pressures within the vacuum system for tetradecylamine.

G. n-Hexadecylamine

The last compound that was analyzed by LP-FFS was n-hexadecylamine ($C_{16}H_{33}NH_2$). The study of hexadecylamine was limited to two experiments, the determination of the laser power index and limit of detection, due to difficulties in introducing the sample vapor to the photolysis chamber.

A sample pressure of only 2×10^{-5} torr was used in the study of the power dependence of CN(B-X) 0,0 fluorescence of photolysis laser energy. A power index of n = 0.6 was obtained. The detection limit (S/N = 2) obtained for hexadecylamine, also based on CN(B-X)

fluorescence at 388.3 nm, was estimated to be ca. 2 x 10^{-6} torr or 41 pmoles.

The detection limit for hexadecylamine represents an improvement in sensitivity over that found for tetradecylamine. This later determination, however, was carried out after the performance of the excimer laser, in terms of pulse energy and operating stability, had been significantly improved. Another change that was made was in the UV-photodiode used to trigger the boxcar averager. Since the last experiments of this type, it was learned that the performance of the UV-photodiode could be improved by the application of a + 9V bias potential to the cathode. A combination of the greater amplitude stability of the laser and the faster response time of the photodiode probably resulted in the reduction of noise observed for the fragment fluorescence signals produced by the laser photolysis of hexadecylamine.

H. LP-FFS: Detection Sensitivity vs. Molecular Weight for Primary Amines

It was of interest to determine how the relative fragment distributions and detection sensitivity would change with changes in molecular weight. As the molecular weight of a molecule increases, there will be less photon energy available for bond dissociation on a per-bond basis. Thus, the possibility exists that significant decreases in sensitivity may arise for larger molecules as excited state fragments are formed less efficiently.

In the case of each of the five primary alkylamines investigated, CN(B-X) fluorescence from the 0,0 transition at 388.3 nm is the most intense emission. Since only one CN fragment can be formed per molecule, by analyzing primary amines of increasing alkyl chain length, one can observe the effect of increasing molecular weight on detection limits directly. The so-called "large-molecule effect," if it is active in this class of compounds, should be manifested by increasing limits of detection, based on CN emission, with increasing molecular weight.

For the primary amines analyzed by LP-FFS, the results indicate that there is a trend toward higher detection limits with increasing molecular weight based on the CN fragment. The detection limits given in Table 8, page 77, are expressed as the uncorrected ionization gauge pressures in units of torr for methyl-, butyl-, hexyl-, and tetradecylamine. The detection limits were found to increase by approximately a factor of 2 for each compound listed in this order. The CN fragment, under the conditions of these experiments, is being formed primarily through the unimolecular dissociation of the alkylamine. Since the increase in amine molecular weight in going to successively heavier primary alkylamines is due solely to the increase in the length of the alkyl chain we are effectively observing a decrease in the fluorescence intensity of CN(B) that reflects the changes in the alkyl portion of the molecule. As chain length increases, a smaller proportion of the absorbed energy appears to be available for the production of CN(B). Conversely, there exists a

greater relative probability that the formation of excited state CH fragments will occur.

The values for detection limits determined for all fragments produced by various amines are given in Table 9. The change in the detection limits for fragments CN and CH produced by butylamine and tetradecylamine is in support of the idea that more CH(A) is formed, at the expense of CN(B), for the heavier alkylamine. In going from butylamine to tetradecylamine, the detection limits for CN increase by a factor of 4 while no increase is seen in the detection limits for CH.

The arguments given above are based on the assumption that the absorptivity of the compounds at the photolysis wavelength is roughly the same and thus that differences in the ability of the compounds to absorb 193-nm photons do not influence their relative detection sensitivity. Table 10 gives the available UV absorption data for each compound. The absorption data provides evidence that all of the amines studied have moderate to strong absorption features in the vicinity of the photolysis wavelength. In the absence of any absorption data for tetradecylamine, it is assumed that tetradecylamine absorbs at 193 nm, given that the absorption spectrum of a primary alkylamine should not drastically vary with changes in the alkyl chain length. The value obtained for the detection limit of tetradecylamine is consistent with this assumption as it follows the trend observed for the primary amines of lower molecular weight.

The variation in detection limits in going from n = 1 to n = 14, where n is number of alkyl carbon atoms, was over a relatively small

Table 9. LP-FFS detection limits.

Compound	Fragment (transition) Wavelength (nm)		
	$CN(B^2\Sigma-X^2\Sigma)(388)$	$CH(A^2\Delta-X^2\pi)(431)$	$NH(A^3\pi-X^3\Sigma)(336)$
$n\text{-}C_4H_9NH_2$	26 pmol	100 pmol	0.3 nmol
$(C_2H_5)_2NH$	44 pmol	-	-
$(C_4H_9)_2NH$	20 pmol	35 pmol	a
$(C_4H_9)_3N$	70 pmol	30 pmol	a
$n\text{-}C_{14}H_{29}NH_2$	100 pmol	120 pmol	0.93 nmol

[a]No detectable emission.

Table 10. UV absorption data for compounds analyzed by LP-FFS.

Compound	Abs Max (nm)	Abs Characteristics at 193 nm	Ref
NH_3	194	ε = 5,700 L/mole-cm	a
CH_3NH_2	215	ε = 500 L/mole-cm	a
n-$C_4H_9NH_2$	174	strong, increasing	b,c
$(C_2H_5)_2NH$	194	ε = 3,000 L/mole-cm	a
n-$C_6H_{13}NH_2$	-	strong, increasing	c
$(C_4H_9)_2NH$	-	mod. strong, decreasing	c
$(C_4H_9)_3N$	-	mod. strong, increasing	c
n-$C_{14}H_{29}NH_2$	-	--	
CH_3CN	274 (ε=0.002)	no absorbance	b,c

[a]Tannenbaum, et al., J. Chem. Phys., 21, 311 (1953).

[b]Organic Electronic Spectroscopic Data, vols. 2-4.

[c]Vapor-phase UV absorption spectra: 250-192 nm scan range, 2.0 abs. units/full-scale, 0.5 nm/sec scan speed.

range, from 6 x 10^{-7} to 4 x 10^{-6} torr, respectively. This represents an increase in detection limits by only a factor of 6.7.

This is a significant result in that the relatively small decrease in sensitivity seen for the analysis of tetradecylamine is a good initial indication that FFS is likely to be applicable to the sensitive analysis of compounds over a broad range of molecular weights.

The large-molecule effect could also be invoked to explain the change seen in n, the power dependence of CN emission intensity on laser fluence. Table 11 lists values of n determined for the five primary alkylamines along with the laser fluences used in each determination. For the first four alkylamines in Table 11, the value of n is smallest (n = ~1) for methylamine, and steadily increases with increasing molecular weight through tetradecylamine (n = 3.2). An average value for the laser fluences used was ca. 3 x 10^{18} photons/cm^2.

Assuming that the same number of photons is involved in the production of CN(B) for each compound, then this trend may indicate a decrease in the saturation of fragment formation processes for reasons that are analogous to those given to explain the data for the detection limits; there is less energy available for each pathway leading to the production of emissive fragments, including CN(B), as the molecular weight increases. If this is the case, then the large-molecule effect may be circumvented by the use of higher laser fluences, within the limits imposed by the condition for maintaining sequential photon absorptions.

Table 11. Values of n, the laser power dependence, for primary alkylamines.

Compound	n	Median Laser Fluence (photons/cm^2) Used in Determination of n
CH_3NH_2	~1	2.5×10^{18}
$C_4H_9NH_2$	1.8	2.8×10^{18}
$C_6H_{13}NH_2$	2	2.5×10^{18}
$C_{14}H_{29}NH_2$	3.2	3×10^{18}
$C_{16}H_{33}NH_2$	0.6	2.7×10^{18}

Alternately, these results may be due to the requirement of a greater number of photons in order to form CN(B) by the alkylamines of higher molecular weight. The possibility that major changes in the multiple-photon fragmentation mechanism for these compounds may occur with changes in the size of the alkyl group cannot be ruled out on the basis of the present data.

Even though changes that were made in the LP-FFS instrumentation detract from the ability to directly compare the results for hexadecylamine to those of the other amines, the final laser photolysis experiment of hexadecylamine still warrants comment.

The detection limit for hexadecylamine (41 pmole) is lower than the detection limit for tetradecylamine (100 pmole). In consideration of the instrumental improvements that were made in the generation and detection of fragment fluorescence, the significance of this result is tentative. However, the implication is that there is no obvious manifestation of the heavy molecule effect between the results for tetradeyl- and hexadecylamine.

The value of the power index for hexadecylamine is anomalous in comparison to those of the other alkylamines (see Table 11). In LP-FFS, moderate to low power indices are desirable as they decrease the extent to which the emission signal varies with pulse-to-pulse changes in energy of the photolysis laser. One can only speculate as to the cause of the reduced dependence of CN(B) fluorescence on laser energy for the heavier amine based on this experiment; either the number of photons required in the multiphoton absorption

is diminished or the absorption process is more highly saturated under the current conditions of photolysis.

I. Dibutylamine, Diethylamine, and Tributylamine

A series of more highly substituted alkylamines was analyzed by LP-FFS in order to assess the effects of amine-substitution, as well as molecular weight, on both fragment fluorescence detection sensitivity and relative fragment intensities.

1. Laser Photolysis

The survey spectra produced upon laser photofragmentation of the single tertiary amine and two secondary amines are shown in Figure 16. No NH(A-X) emission was detectable under the experimental conditions used to acquire each survey spectrum. As was seen for the primary amines, the most intense fragment emission was due to the CN(B-X)0,0 transition at 388.3 nm.

In the absence of any rearrangement process, no NH fluorescence is expected for the laser photolysis of tertiary alkylamines as NH cannot be directly produced by cleavage of the C-N bonds. In the case of the secondary amines, however, the absence of any detectable NH may indicate either a loss in the efficiency with which NH(A) is produced (a direct consequence of the "large-molecule effect") or the lack of a spectroscopic (or photochemical) channel for its formation in the laser photolysis of these parent compounds at 193 nm.

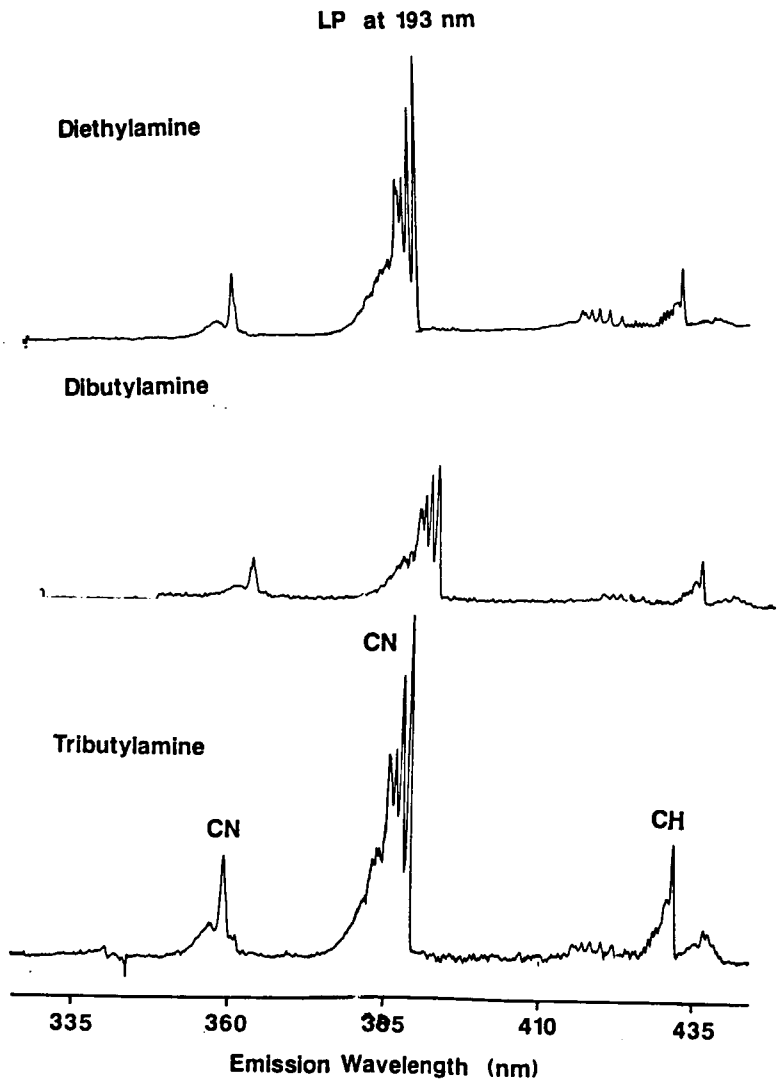

Figure 16. LP-FFS emission spectra of diethylamine, dibutylamine, and tributylamine.

Diethyl- and dibutylamine yielded laser power indices of nearly equal values, n = 1.2 and 1.3, respectively. The value of n for dibutylamine was based on the entire range for the power dependence plot; it changed in value from 1.6 for laser energies of 50-80 mJ/pulse to 1.2 for energies of 80-100 mJ/pulse. The result obtained for tributylamine was n = 2.2. In the absence of any other relevant data, these results could mean either that the rate-determining photon absorption processes involved in the formation of CN(B) are effectively less strongly saturated for the tertiary amine than in the case of either of the two secondary amines or that more photons are required to produce CN(B) from the tertiary amine.

The results of the limit of detection studies for all three compounds were similar and are summarized in Table 8, page 77. For the two secondary amines, dibutylamine yielded a slightly lower detection limit than did diethylamine. However, given that the reported values were not corrected for pressure gauge response, the significance of this difference is questionable. The detection limit for tributylamine was the highest of the three compounds, 3×10^{-6} torr or 9×10^{10} molecules/cm^3 (S/N = 2) or 70 pmoles. Again, the difference between it and the lowest limit of detection was small and represents an increase by only a factor of 3.5.

The results of the linear dynamic range studies for these amines are summarized in Table 8, page 77. For each compound, the CN emission signal was linear in sample pressure over the entire pressure range investigated. The percent relative standard deviation obtained for the

slopes of the calibration curves by linear regression analysis were 4.4%, 7.4%, and 3.8% RSD for diethyl-, dibutyl-, and tributylamine, respectively.

The results of the precision studies of the three compounds are also given in Table 8, page 77; the values for RSD are similar to each other, with the range in relative standard deviations spread only from 4.6 to 6.8%. The lowest variation in signal reproducibility was obtained for tributylamine. This result is not expected since, of the three compounds, tributylamine exhibited the greatest laser power index and thus should be the most susceptible to variations in emission intensity due to pulse-to-pulse fluctuations in laser power.

J. LP-FFS: Detection Sensitivity vs. Alkyl-Substitution

Data for the limits of detection obtained for the more highly substituted alkylamines analyzed by LP-FFS are given in Table 8, page 77. A decrease in detection limits by a factor of ~1.5 was seen in going from butylamine to dibutylamine. In going from a primary amine to a secondary amine of the same molecular weight (from butylamine to diethylamine) an increase in detection limits by about the same amount was observed.

The small difference between the detection limits obtained for butyl- and dibutylamine may not be significant. The comparison was made between two compounds that are both relatively strong absorbers of 1933-nm radiation and uncalibrated pressures were used in the assessment of these data. The same can be said for the comparison of

detection limits for butylamine and diethylamine. From these data it can neither be concluded that the process of formation of excited fragments is more efficient for dialkylamines than for primary alkylamines, nor that the secondary amine of higher molecular weight will necessarily have a higher detection limit than the corresponding primary alkylamine.

A comparison of the data for butylamine and tributylamine reveals an increase in the detection limit for tributylamine by a factor of 3 over that obtained for butylamine. If one assumes the difference in the detection limits for butylamine and tributylamine to be significant, then the problem becomes one of identifying the cause for that difference. In comparing the UV absorption data for the two compounds it can be seen that tributylamine is not as strong an absorber of 193 nm-radiation as is butylamine. The loss of sensitivity may be due to the smaller absorption cross-section of tributylamine or to a molecular weight effect. In this case, the effect that increasing N-substitution has on altering the UV absorption characteristics of the amines could be the predominant influence in determining the relative sensitivity.

The limits of detection obtained by LP-FFS including excited fragments other than CN are given in Table 9, page 97. The general trend observed is that, as the alkyl contribution to the molecular weight of these amines increases, the limits of detection for the NH and CN fragments increase relative to those for the CH fragment. This result is exactly what one should expect based on the arguments put

forth to explain the data for the detection limits of the n-alkylamines. The results for butyl- and tributylamine are used to assess the effect of increasing N-alkyl substitution on this trend. In going from the primary to the tertiary butylamine, the fragment fluorescence due to CN exhibits a 3-fold increase in detection limit, whereas the CH signal shows a decrease in limit of detection by a factor of ca. 3.5. A comparison of relative fragment fluorescence intensities for two primary alkylamines shows a similar trend. In going from an alkyl-chain length of n = 4 to n = 14 for butylamine and tetradecylamine, respectively, the detection limits for CN and NH increase by roughly a factor of 4 while that for CH remains unchanged.

K. Acetonitrile

1. Electron Impact

The electron impact-fragmentation fluorescence spectrum of acetonitrile is shown in Figure 17. Three emissive fragments were observed in the spectral region ranging from 300 to 500 nm. Listed in decreasing order of their relative intensities, they are CN(B), CH(A), and H. Under conditions given in Table 2, page 38, for this experiment the maximum peak height due to CN(B-X)0,0 fluorescence was ~2,000 cps.

The limit of detection was found to be 6×10^{-7} torr or 2×10^{10} molecules/cm^3 (S/N = 2). Absolute detection limits of 5.2 ng or 0.13 nmole were calculated. The corresponding uncorrected pressure was 4×10^{-7} torr. The CN(B) emission at ~388 nm was linear in acetonitrile pressure over 2 decades for the slope of the calibration plot

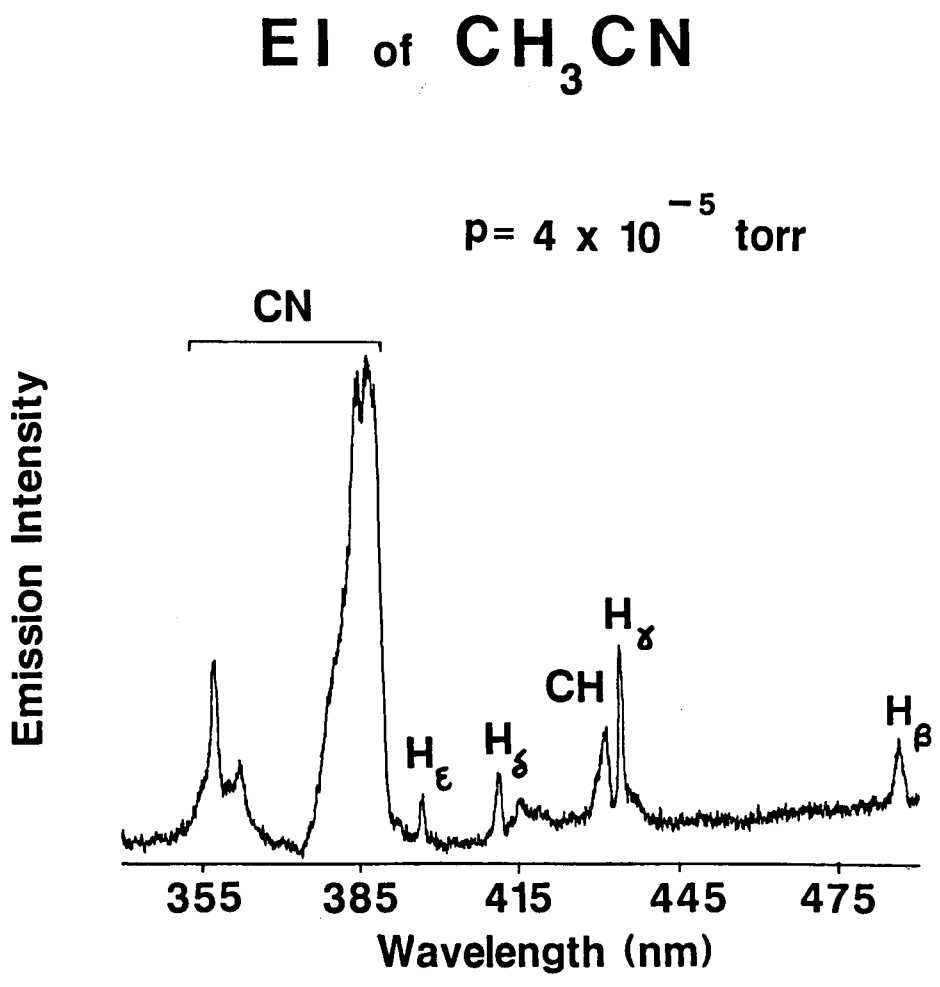

Figure 17. EI-FFS emission spectra of acetonitrile.

(RSD = 2.3% and r = 0.9980). A negative deviation in linearity was seen for the high pressure extreme from approximately 1 x 10^{-4} to 3 x 10^{-4} torr.

The relative standard deviation for CN(B-X)0,0 fluorescence was estimated to be 1.2% for n = 6 at a pressure of ca. 2 x 10^{-6} torr.

2. Laser Photolysis

No detectable fragment fluorescence was observed when acetonitrile was subjected to laser-photofragmentation under experimental conditions similar to those used for the laser photolysis of the amine compounds. The lack of an absorption band (see Table 10, page 98) in the vicinity of the UV-photolysis wavelength for acetonitrile is attributed as being the cause of this result. This case is important, however, in that it demonstrates the potential for analytical selectivity available through laser photolysis-fragmentation as opposed to electron impact-fragmentation techniques.

Electron impact is a universal fragmentation technique that produces both neutral and charged species. Laser photolytic techniques, on the other hand, are inherently selective because they depend upon the absorption of photons of specific wavelengths. For relatively low photon fluences, i.e., for sequential absorption processes, absorption occurs only for those compounds having electronic absorption bands corresponding to the wavelength of the photolysis laser. The inherent selectivity of UV laser photolysis is illustrated in a case whereby attempts to produce excited state CN radicals from

fumaronitrile using 248-nm excimer laser radiation were unsuccessful (53). Fumaronitrile does not absorb appreciably at 248 nm.

In addition, whether fragments ultimately will be formed in a particular experiment depends upon at least three more intrinsic characteristics of the parent molecule, 1) the lifetimes of the electronically excited precursor molecule or molecular ion, 2) the total number of photons required to produce an emissive fragment, and 3) optical selection rules. Electron-impact fragmentation techniques generally use electron energies that are greatly in excess of the energies necessary to form and electronically excite fragments, and excitation can be independent of optical selection rules. Thus, there exists a larger number of restrictions which govern the production of emissive fragments by laser photolysis than electron impact.

One of the most significant analytical advantages of LP- over EI-FFS is the application of LP-FFS to the analysis of mixtures without prior chemical separation. This aspect of LP-FFS is founded on the ability to selectively photolyze individual constituents based on the differences in their absorption spectra.

L. Two-Laser Experiments

1. Initial Studies

a. n-Butylamine. The first attempts at LIF with the use of a probe laser were on the CN radical produced by the laser photolysis of n-butylamine. With the fluorescence collection lenses and emission monochromator optimized for detection of CN(B-X)0,0 fluorescence at

388.3 nm, the two lasers and boxcar averager were synchronized and the excitation wavelength was scanned through the $\Delta v = 0$ series from 388.5-385.5 nm (53,56). No difference was seen between the excitation spectrum at a butylamine pressure of 1×10^{-4} torr and the blank excitation spectrum (no sample) for the experiment other than the presence of a relatively constant background signal that was attributed to CN fluorescence induced by the photolysis laser.

Subsequent resonance fluorescence spectra (the monochromator was scanned over the same transition that was probed) of the 0,0 transition revealed no increase in the intensity of CN(B-X) fluorescence at this vibronic transition with probe laser excitation.

One possible cause for the lack of any detectable enhancement of fluorescence under these experimental conditions could lie in the production of fragments by laser photolysis. Per-pulse laser fluences estimated for the photolysis laser in these studies are on the order of 3×10^{18} photons/cm^2 (71). This value is three orders of magnitude greater than the laser fluences reported for a similar "photolysis-probe" LIF experiment of the CN radical by Xie, et al. (53). Given the relative intensity of the photolysis laser fluence used in the two experiments, conceivably, the majority of CN radicals formed are in excited electronic states and thus are not available for excitation.

In order to test this idea, the same excitation experiment was repeated under milder photolysis conditions. The pulse energy of the photolysis laser was reduced by about 45% or to the lowest energy setting for stable operation of the laser. There was no change in the

overall appearance of the excitation spectrum of this experiment from that of the spectrum acquired using a higher laser energy. Not surprisingly, the magnitude of the intensity of the background fluorescence was diminished somewhat given the nonlinear dependence of CN fluorescence intensity on photolysis laser energy.

b. LIF: Cu. As an aid in interpreting the results of the butylamine experiments, the two-laser experiments performed previously in this laboratory on the copper chelate, bis (hexafluoroacetylacetonato) copper II, or Cu $(hfa)_2 \cdot 2H_2O$, were repeated. These earlier studies indicated that enhancement of emission from the bare Cu atom could be achieved readily with probe laser excitation (67,71). The relative success of the copper experiment, carried out in a manner similar to the LIF experiments of CN, would possibly reveal whether any problems existed in the way the latter experiments were being performed.

With the exception of the excitation wavelength, the copper experiments, in terms of synchronization of the lasers and boxcar averager, were very similar to the CN experiments (see Table 4, page 70). Since the optimal excitation wavelength was already known to be 324.75 nm, corresponding to the resonant excitation of $Cu(^2P_{1/2}-^2S_{1/2})$ emission, no excitation experiment was performed. Instead, an emission spectrum of this transition was acquired with and without the probe laser beam.

An increase in the intensity of the Cu emission of the two-laser emission spectrum of a factor of 3 was seen over that of the one-laser emission spectrum.

The copper chelate was used to optimize the two-laser experiment by maximizing the LIF signal of Cu ($^2P_{1/2}$-$^2S_{1/2}$). The procedure consisted of optimizing the two-laser delay time, the boxcar delay time and the position of the probe laser beam. Some results of these procedures are described below.

In the course of the optimization experiments, it was learned that the same photolysis laser energy should be used in carrying out gate scans for t^{max}_F and t^{max}_s. These quantities varied as a function of laser energy probably due to a like dependence of the photodiode response time, the result was that the boxcar gate scans were affected by any change in the pulse energy of the photolysis laser. It was also learned that the variable delay circuit could drift by an estimated ± 20 ns while the system was under operation. In order to be assured that the probe laser pulse followed the photolysis laser pulse, but that the two lasers were firing nearly simultaneously, a minimum two-laser delay time of approximately 20 ns should be used.

A boxcar gate scan of the Cu emission for the two-laser experiment was carried out to determine the optimal delay time for the boxcar averager. The LIF decay curve thus produced indicated the presence of an emission maximum occurring 2-4 ns beyond the time of the maximum probe laser scattered light signal, t^{max}_s. The boxcar delay was therefore adjusted to follow t^{max}_s by 2ns.

The Cu emission intensity was not found to be strongly dependent on the position of the probe laser beam nor was any improvement in the signal made by carefully adjusting the beam. This result implied that

the probe beam alignment with respect to the focused photolysis beam and sample introduction tube was already nearly optimal and also that the Cu ($^2S_{1/2} \rightarrow {}^2P_{1/2}$) transition could be optically saturated at the level of probe laser fluence used.

Following the optimization procedures described above, the LIF emission experiments of Cu were repeated. The two-laser emission was found to be more intense than the one-laser emission by a factor of 28, an order of magnitude improvement from the results of the initial experiments with Cu $(hfa)_2 \cdot 2H_2O$.

2. LIF: CN

a. n-Butylamine. The LIF experiments with the copper chelate were followed directly by another attempt to excite additional fluorescence from CN. The only change that was made between the two experiments (other than the necessary change in the excitation wavelength) was the use of a longer boxcar delay time. The longer fluorescence lifetime of CN(B) than that of Cu ($^2P_{1/2}$) (~65 ns vs. ~20 ns (71)) enabled the use of time-based discrimination against the scattered light signal. At a boxcar delay time of 24 ns (relative to t^{max}, obtained by scanning the boxcar delay time by hand), the intensity of fluorescence produced by the photolysis laser was still significant but the scattered light from the probe laser had decayed by ~80%. Thus the boxcar sensitivity (amplifier gain) was increased for the subsequent acquisition of an excitation spectrum. Apparently some excitation of ground-state CN was achieved by this experiment. Weakly intense peaks (S/N = ~2) that

occurred at the same excitation wavelengths as those in the LIF excitation spectrum of Xie, et al. (53) were observed. The LIF excitation experiment was immediately followed by the acquisition of LIF emission spectra at three different excitation wavelengths. Since for CN(B-X) three vibronic transitions of the $\Delta v = 0$ sequence are observed in emission with relatively high intensities, the probe laser wavelength was tuned to correspond to each of these transitions and emission spectra including all three emission bands were acquired. Thus, the effect of excitation of a particular transition could be observed at resonant as well as nonresonant emission bands. The only excitation wavelength that corresponded to a peak in the excitation spectrum was 386.2 nm, corresponding to the (2,2) transition. No change in the fluorescence intensity was observed for either the resonant or off-resonant transitions.

There are differences between the LIF excitation experiment of this work and the one published by Xie, et al. that could be critical to the relative success of the two experiments. In the published spectrum, the parent compound, fumaronitrile, was at a pressure of 1-10 x 10^{-3} torr. Although the authors state that their experiments were carried out under "collision-free conditions," the pressures used were substantially higher (X10 to X100) than the pressure of butylamine in this work. Collision rates under the conditions of Xie, et al., may be low but are not nonexistent and are still higher than those estimated for the butylamine experiment (~700 s^{-1}). In general, collisional relaxation rates, providing a pathway between rotationally and

vibrationally excited states and the $v' = 0$, CN(B) state from which emission is observed, are greater at higher pressures.

The two excitation experiments cannot be compared on the basis of sample pressure alone. Both butylamine and fumaronitrile absorb 193-nm photons to yield CN radicals but the efficiencies for production probably differ. The structure of fumaronitrile (trans-1,2-dicyanoethylene) probably favors the production of CN radicals more so than does that of n-butylamine since two CN radicals per molecule, formed by the rupture of just one C-C band per radical, are possible for fumaronitrile. In the case of n-butylamine, 5 bonds must be broken within the amine functional group of the molecule to form one CN radical per molecule. Given that the thermodynamics of bond dissociation for both molecules are equally favorable, the fumaronitrile is likely to yield a greater partial pressure of CN radicals than butylamine.

There are at least two fundamental differences in the way the two LIF excitation experiments were performed that could affect the sensitivity for LIF detection of CN(X). Xie, et al. used a much longer two-laser delay time (250-500 ns) thus potentially allowing the LIF detection of CN(X) formed by the decay of CN(B) as well as other excited electronic states of CN produced by the photolysis laser pulse. However, the importance of the contribution of LIF from this component to the overall signal level cannot be readily assessed without comparing the interrogation volumes of the two systems as the diffusion of ground-state radicals in to and out of this region may become important at longer delay times.

The second difference in the experimental design of the two systems was the use of an interference filter for the detection of fluorescence by Xie, et al. and an emission monochromator in this work. The spectral band pass of interference filters is typically on the order of nanometers, thus permitting the emission from more than one rovibrational transition to be observed. The ultimate choice of spectral bandpass may be influenced by the extent to which stray or scattered source radiation is reduced by light baffling techniques regardless of whether an interference filter or a monochromator is used. The spectral bandpass of the monochromator used in this work was relatively narrow, ~0.1 nm, as the measures taken to baffle scattered radiation of the photolysis laser within the vacuum chamber (71) were not effective in reducing scattered light from the probe laser. The sensitivity of LIF detection in this work could have been limited by the low throughput of the emission monochromator.

3. LIF: NH

a. Methylamine. Methylamine was chosen for the initial attempts at LIF of the NH radical instead of butylamine because of the more intense NH(A-X) fluorescence observed for that compound in one-laser experiments. Slightly longer delay times were established for the investigations of NH by LIF because of the relatively long lifetime of the $A^3\pi$ state (~430 ns). A two-laser delay time of approximately 35 ns was used, thus allowing greater assurance of the firing of the two lasers in the proper sequence, without either a significant reduction

of detectable background fluorescence or appreciable decay of the NH fragment to the ground state. A relative boxcar delay time of 30 ns was used in order to discriminate against the scattered probe laser radiation which was of a relatively short pulse duration.

Three different LIF excitation spectra were acquired. The NH(A-X)0,0 band at 336.1 nm was monitored in emission while the excitation wavelength was scanned through the region of the 0,0 Q-head (47), 336.2-333.0 nm. A second similar LIF excitation scan was through the (1,1) and (0,0) bandheads (337.2-335.0 nm) while the (1,1) transition was monitored in emission. A third and final spectrum was identical to the first except that the excitation range was extended to include excitation through the (1,1) bandhead as well. No excitation was apparent for any of these spectra. Not surprisingly, LIF emission spectra yielded similar results. There was no change in the intensities of emissions observed at 336 and 337 nm as the result of probing either the 0,0 or 1,1 transitions.

As for the LIF experiments on the CN radical, some important experimental differences exist between this work and previous LIF studies on NH (45,47). The very large total pressures used in the studies of Fairchild, et al. (45) and Garland, et al. (47) (see p. 18) may account for the reported success of performing off-resonant excitation. For both studies the spectral bandpass of the emission monochromator was 1-2 nm.

b. n-Tetradecylamine. One of the longer-chain alkylamines, tetradecylamine, was used for a final LIF excitation experiment on the

NH radical. This choice of sample was made on the grounds that, for a larger molecule, less energy would be available to produce NH in electronically excited states with possibly a higher proportion being formed in the ground state.

The results of this experiment were unchanged from those of the two-laser experiment involving methylamine. No excitation was apparent from the excitation of NH through the 0,0 bandhead while the 0,0 band was monitored in emission. The emission spectrum with resonant excitation at 336 nm was similarly unchanged as no increase in fluorescence was observed between the one-laser and two-laser spectra.

4. LIF: CH

a. n-Butylamine. The final LIF excitation experiment was on the third fragment produced by the one-laser photolysis of the alkylamines. The experiment was based on the work of Becker, et al. (72) who carried out LIF excitation of $CH(A^2\Delta\text{-}X^2\pi)$ fluorescence in a microwave discharge of acetylene (1×10^{-3} torr with a collision gas of He or Ar). Probe laser excitation through (0,0) Q and R branches, including resonant excitation of the (0,0) Q-head at 431.4 nm was observed.

For the LIF excitation of CH(X) produced by the laser photolysis of butylamine, no change in background fluorescence was observed through the range of excitation wavelengths used (433.0-428.0 nm). The experimental conditions were very similar to those of the "optimized" two-laser experiments for the CN and NH radicals; a much lower probe laser energy was obtained in this experiment, however, because only ~20% of the beam was transmitted by the beam-steering optics.

M. Summary and Conclusions

1. Comparison of EI- and LP-FFS

a. Sensitivity. The limit of detection for ammonia (fragment: NH) determined by LP-FFS was four times lower than the detection limit determined by EI-FFS. For methylamine, the comparison between the two techniques must be based on two different fragments, H_s for EI, and CN for LP-FFS. The detection limit determined by LP-FFS was approximately fifteen times lower than that determined by EI-FFS. Based on these data, LP-FFS appears to be the more sensitive method of analysis of the two techniques.

There may be several reasons for the ostensibly higher sensitivity of LP-FFS; there are undoubtedly instrumental differences that affect the relative sensitivity of the two techniques, e.g., pulsed photons with gated detection and signal averaging, vs., dc electrons with photon-counting. Of a more fundamental nature is the production of fewer emissive fragments by LP; thus, the energy of the photolysis laser may be distributed among fewer fragmentation pathways than in electron impact.

b. Linear Dynamic Range. The linear dynamic ranges offered by both techniques are comparable (2-3 orders of magnitude). In these studies, the linearity of EI-FFS was typically limited at high pressures by poisoning of the thoriated iridium filament (as indicated by nonrecovery of signal levels expected for lower pressures). However, the subsequent use of tungsten filaments has resulted in a

substantial improvement of this problem (69). Both techniques exhibited negative deviations in linearity at higher pressures, presumably due to an increase in fluorescence quenching and chemical reactions due to bimolecular collisions. In LP-FFS linearity can potentially be extended at lower pressures by taking measures to correct for the per-pulse variation in the laser energy.

c. Precision. There is a clear superiority in the reproducibiity in measurements made by EI-FFS over LP-FFS. The values determined for precision by these studies were consistent with those of previous precision studies by EI- (69) and LP-FFS (71). The difference between the two techniques may be largely attributable to the inherent stability of dc electron beam currents as opposed to the relatively large variation in the pulse-to-pulse energy of the excimer laser (± ~6%).

d. Selectivity. An advantage of LP-FFS over EI-FFS is the potential selectivity it offers based on the differences in the absorption spectra of compounds. Electron-impact at electron energies of 100 eV is a "universal" fragmentation technique. No possibiity exists for selectively fragmenting molecules by EI-FFS without the use of chemical separation techniques.

2. Two-Laser Experiments

There are three possible reasons for the lack of any detectable probe-laser-induced fluorescence from the molecular fragments investigated by this study. The first and perhaps the most plausible

reason is that the ground-state fragments are not being efficiently excited by the probe laser. Given that the two-laser experiment produces a significant enhancement of Cu emission under essentially the same experimental conditions, the discrepancy between the results of the two experiments is likely to be attributable to fundamental differences between molecular and atomic spectra.

For atomic species, absorption and emission spectra involve only transitions of electrons between electronic energy levels, whereas, in molecular spectra, transitions between electronic states may be accompanied by transitions between rotational and vibrational energy levels. The inefficiency in the excitation of molecular fragments could thus be caused by the inability to excite more than a fraction of the ground state fragments at any particular wavelength; ground-state fragments, when formed by the photolysis laser pulse, populate a distribution of vibrational and rotational energy levels. Evidence for the production of rovibrationally hot ground-state fragments in these experiments is provided by the single excitation spectrum of CN in which excitation of individual rotational transitions of $v'' = 0$ and 1 was evident.

The second possible explanation for the results of the two-laser experiments is related to the inefficient collection of the probe-laser-induced fluorescence. The spatial arrangement of the two laser beams is such that the pathlength of the laser/sample interaction region is maximal. However, further changes in the relative beam positions and cross-sectional areas may be needed for maximal LIF. The

progress of such experiments is hindered by the lack of a strong or, as in the case of this work, a detectable LIF signal. The optimization of the laser beams is also impeded by the presence of a very large background signal due to scattered probe laser light, the intensity of which changes depending on the size and position of the probe laser beam.

An increase in the fluorescence collection efficiency could also be gained if a larger spectral bandpass were used. These experiments were restricted to the use of a relatively narrow spectral bandpass necessitated by the magnitude of the scattered laser light signal.

More effective measures to baffle the scattering of photons from the probe laser would facilitate the optimization of the spatial parameters of the two lasers as well as the increase of optical throughput, and hence sensitivity, by reducing the scattered light signal to more manageable levels.

A third possibility that may explain these results could be that not enough fragments are being produced in ground electronic states. Two excitation experiments were performed to assess this idea: the LIF excitation spectrum of CN at a reduced photolysis laser energy, and the LIF excitation spectrum of NH produced from the heavier molecule, tetradecylamine. The results of these experiments indicate that apparently no significant increase in the relative abundances of these fragments in the ground electronic state was obtained.

An important premise for the use of LIF techniques in conjunction with FFS is that fragments in excited electronic states from which

fluorescence may be observed are produced with efficiencies of less than 100% by the fragmentation process. However, at the very high photon fluences that were used in laser photolysis, it is not unreasonable to assume that fragments were formed in excited electronic states other than those observed in fluorescence (38,40,49,53) and that these processes compete with photochemical pathways leading to the production of ground state fragments. If, under these conditions of photolysis, this is the case, then attempts to increase the relative abundance of the ground-state fragments may not necessarily succeed.

REFERENCES

REFERENCES

1. H. H. Willard, L. L. Merritt Jr., J. A. Dean, and F. A. Settle Jr., "Instrumental Methods of Analysis," 6th ed., Wadsworth Publishing Company, Belmont, California, 1981.

2. E. L. Wehry, in R. A. Minear and L. H. Keith, Eds., "Water Analysis," Academic Press, Inc., Orlando, Florida, 1984, ch. 4.

3. E. L. Wehry, in G. G. Guilbault, Ed., "Practical Fluorescence: Theory, Methods, and Techniques," Dekker, New York, NY, 1973, ch. 3.

4. W. R. Seitz, CRC Crit. Rev. Anal. Chem., 8, 367 (1980).

5. J. B. Halpern and X. Tang, Chem. Phys. Lett., 122, 294 (1985).

6. E. Tannenbaum, E. M. Coffin, and A. J. Harrison, J. Chem. Phys., 21, 311 (1953).

7. J. I. Peterson, R. V. Fitzgerald, and D. K. Buckhold, Anal. Chem., 56, 62 (1984).

8. S. I. Mho and E. S. Yeung, Anal. Chem., 57, 2253 (1985).

9. R. N. Perutz, Chem. Rev., 85, 77 (1985).

10. H. Reisler, M. Mangir, and C. Wittig, in C. B. Moore, Ed., "Chemical and Biochemical Applications of Lasers," Academic Press, New York, NY, 1980, 5, 139.

11. R. W. B. Pearse and A. G. Gaydon, "The Identification of Molecular Spectra," Wiley, New York, NY, 1963.

12. S. N. Suchard, "Spectroscopic Data," Plenum, New York, NY, 1975.

13. C. A. Gierczak, M. A. Heindorf, and J. Allison, Anal. Chem., 56, 2966 (1984).

14. M. L. Robin, G. K. Schweitzer, and E. L. Wehry, Appl. Spectrosc. Rev., 17, 165 (1981).

15. H. Bukert and F. W. Froben, J. Phys. Chem., 75, 769 (1971).

16. H. D. Morgan and J. E. Mentall, J. Chem. Phys., 60, 4734 (1974).

17. T. Sato, F. Shibata, and T. Goto, Chem. Phys., 108, 147 (1986).

18. K. Fukui, I. Fujita, and K. Kuwata, Bull. Chem. Soc. Jpn., 45, 2278 (1972).

19. I. Fujita, Z. Phys. Chem. N. F., 149, 17 (1986).

20. I. Fujita, Z. Phys. Chem. N. F., 136, 187 (1983).

21. C. A. F. Johnson, J. E. Parker, and H. P. Flitman, J. Chem. Soc. Perkin Trans. II, 903 (1982).

22. T. Sawada and H. Kamada, Bull. Chem. Soc. Jpn., 43, 331 (1970).

23. W. H. Smith, J. Chem. Phys, 51, 520 (1969).

24. I. Tokue and M. Iwai, Chem. Phys., 52, 47 (1980).

25. K. Fukui, I. Fujita, and K. Kuwata, J. Phys. Chem., 81, 1252 (1977).

26. I. Tokue, I. Nishiyama, and K. Kuchitsu, Chem. Phys. Lett., 35, 69 (1975).

27. I. Tokue, T. Urisa, and K. Kuchitsu, J. Photochem., 3, 273 (1974-75).

28. I. Tokue, A. Fujimaki, and Y. Ito, J. Phys. Chem., 88, 6250 (1984).

29. D. A. Radspinner and E. L. Wehry, Talanta, 34, 963 (1987).

30. E. L. Wehry, R. Hohmann, J. K. Gates, L. F. Guilbault, P. M. Johnson, J. S. Schendel, and D. A. Radspinner, Appl. Opt., 26, 3559 (1987).

31. G. K. Schweitzer and I. Ishii, Spectrosc. Lett., 17, 713 (1984).

32. H. M. Gillespie and R. J. Donovan, Ann. Rep. Progr. Chem., 77C, 173 (1980).

33. H. Reisler, G. Radhakrishnan, D. Sumida, J. Pfab, J. S. Chow, I. Nadler, and C. Wittig, Isr. J. Chem., 24, 259 (1984).

34. A. Gedanken, M. B. Robin, and N. A. Kuebler, J. Phys. Chem., 86, 4096 (1982).

35. W. Demtroder, "Laser Spectroscopy, Basic Concepts and Instrumentation," Springer-Verlag, New York, NY, 1982.

36. D. M. Friedrich, J. Chem. Ed., 59, 472 (1982).

37. D. M. Lubman and M. N. Kronick, Anal. Chem., 54, 660 (1982).

38. V. M. Donnelly, A. P. Baronavski, and J. R. MacDonald, Chem. Phys., 43, 271 (1979).

39. R. D. Kenner, F. Rohrer, and F. Stuhl, J. Chem. Phys., 86, 2036 (1987).

40. R. D. Bower, M. T. Jacoby, and J. A. Blauer, J. Chem. Phys., 86, 1954 (1987).

41. H. K. Haak and F. Stuhl, J. Phys. Chem., 88, 2201 (1984).

42. T. Ni, S. Yu, X. Ma, and F. Kong, Chem. Phys. Lett., 126, 413 (1986).

43. A. Hofzumahaus and F. Stuhl, J. Chem. Phys., 82, 5519 (1985).

44. R. D. Kenner, F. Rohrer, and F. Stuhl, Chem. Phys. Lett., 116, 374 (1985).

45. P. W. Fairchild, G. P. Smith, D. R. Crosley, and J. B. Jeffries, Chem. Phys. Lett., 107, 181 (1984).

46. V. M. Donnelly, A. P. Baronavski, and J. R. MacDonald, Chem. Phys., 43, 271 (1979).

47. N. L. Garland, J. B. Jeffries, D. R. Crosley, G. P. Smith, and R. A. Copeland, J. Chem. Phys., 84, 4970 (1986).

48. N. Nishi, H. Shinohara, and I. Hanazaki, Chem. Phys. Lett., 73, 473 (1980).

49. H. K. Haak and F. Stuhl, J. Phys. Chem., 88, 3627 (1984).

50. L. C. Lee and W. K. Bischel, J. Appl. Phys., 53, 203 (1982).

51. B. B. Craig, W. L. Faust, and R. G. Weiss, J. Chem. Phys., 79, 1286 (1983).

52. B. B. Craig and W. L. Faust, J. Phys. Chem., 87, 4568 (1983).

53. X. Xie, V. R. McCrary, J. B. Halpern, E. Pugh, and W. M. Jackson, J. Phys. Chem., 90, 2670 (1986).

54. S. Hay, F. Shokoohi, S. Callister, and C. Wittig, Chem. Phys. Lett., 118, 6 (1985).

55. M. A. O'Halloran, H. Joswig, and R. N. Zare, J. Chem. Phys., 87, 303 (1987).

56. I. Nadler, J. Pfab, G. Radhakrishnan, H. Reisler, and C. Wittig, J. Chem. Phys., 79, 2088 (1983).

57. I. Nadler, J. Pfab, H. Reisler, and C. Wittig, J. Chem. Phys., 81, 653 (1984).

58. W. M. Jackson, J. Chem. Phys., 61, 4177 (1974).

59. H. Kawazumi and T. Ogawa, Chem. Lett., 925 (1985).

60. M. A. Johnson, M. L. Alexander, I. Hertel, and W. C. Lineberger, Chem. Phys. Lett., 105, 374 (1984).

61. J. B. Halpern, W. M. Jackson, and V. McCrary, Appl. Opt., 18, 590 (1979).

62. V. M. Donnelly and R. F. Karlicek, J. Appl. Phys., 53, 6399 (1982).

63. R. C. Oldenborg and S. L. Baughcum, Anal. Chem., 58, 1430 (1986).

64. S. R. Long, R. C. Sausa, and A. W. Miziolek, Chem. Phys. Lett., 117, 505 (1985).

65. J. Schendel, R. Hohmann, and E. L. Wehry, Appl. Spectrosc., 41, 640 (1987).

66. R. C. Sausa, A. J. Alfano, and A. W. Miziolek, Appl. Opt., 26, 3588 (1987).

67. J. Schendel and E. L. Wehry, Anal. Chem., 60, 1759 (1988).

68. T. Papenbrock and F. Stuhl, in G. Angeletti and G. Restelli, Eds., "Physico-Chemical Behavior of Atmospheric Pollutants, Proceedings of the Fourth European Symposium," Stresa, Italy, Sept. 1986, D. Reidel, Dordrecht (1987).

69. L. F. Guilbault, Ph.D. dissertation, University of Tennessee, Knoxville, TN (1988).

70. P. W. Erdman and E. C. Zipf, Rev. Sci. Instrum., 53, 225 (1982).

71. J. Schendel, Ph.D. dissertation, University of Tennessee, Knoxville, TN (1987).

72. K. H. Becker, H. H. Brenig, and T. Tatarczyk, Chem. Phys. Lett., 71, 242 (1980).

APPENDIX

Table A-1. Values for two-laser delay time as measured by two different methods: A dual-trace oscilloscope and the boxcar gate scanner.

Exp. No.	Two-Laser Delay Time (ns)	
	Boxcar Gate Scan	Oscilloscope
1	425	420
2	360	355
3	270	260
4	204	185
5	140	125
6	80	70
7	20	0
8	0	-15

VITA

Jane Katherine Gates Jinkins was born in Durham, North Carolina, in the hospital where her mother began her career as a registered nurse, and was reared on her family's farm in rural Orange County.

Ms. Jinkins graduated from Chatham Hall, Chatham, Virginia, in June 1977. She received her Bachelor's degree in Environmental Engineering from the School of Public Health, University of North Carolina-Chapel Hill, in August 1982. In September of that year she joined the Department of Chemistry at The University of Tennessee, Knoxville, as a graduate teaching assistant.

Ms. Jinkins has presented a paper at the 1987 Pittsburgh Conference and published a paper in Applied Optics.

In June 1988, Ms. Jinkins was married to Robert M. Jinkins of Wappingers Falls, New York. Ms. Jinkins has accepted a position with the IBM Corporation.